Volume 29 | ANTARCTIC RESEARCH SERIES

Upper Atmosphere Research in Antarctica

L. J. Lanzerotti and C. G. Park, Editors

CHAPTER 5. CONTROLLED WAVE-PARTICLE INTERACTION EXPERIMENTS

R. A. HELLIWELL AND J. P. KATSUFRAKIS

Radioscience Laboratory, Stanford University, Stanford, California 94305

CONTENTS

1. INTRODUCTION

In this chapter we describe the use of controlled VLF waves to conduct wave-particle interaction experiments on the magnetosphere. The test signals are generated by a transmitter located at Siple Station, Antarctica (75°56'S, 85°45'W). (Pictures of Siple Station, 1973, are shown in Plates 1.1, 1.2, and 1.3.)

Why do we need a controlled VLF source when lightning-generated whistlers provide so much information? We have seen in chapter 4 how whistlers can be used to measure the path latitude and equatorial electron concentration. Whistlers in turn trigger emissions that are evidence of wave-particle interaction. However, for quantitative studies the lightning impulse is critically deficient in several respects. Its spectrum and location are difficult to obtain, and its rate of occurrence is irregular. More important is the fact that the lightning impulse cannot be readily controlled. As will be seen in this chapter, many of the significant new phenomena owe their discovery to the availability of a repeatable, precisely timed coherent wave train of adjustable frequency. On the other hand, the lightning impulse, or sferic, is a powerful signal that provides broadband information not easily obtained from a controlled source. Thus sferic and VLF transmitter form a complementary pair for the study of wave-particle interactions in the magnetosphere.

Before discussing technical aspects of the experiments we should understand why they are being conducted at Siple Station, Antarctica. Four necessary conditions were established for the proposed controlled experiments. They are (1) a VLF radiated power of the order of 1 kW, (2) proximity to the plasmapause (near $L = 4$), (3) an accessible magnetic conjugate point, and (4) year-round operation. Because the free space wavelengths of the radiation are unusually long (of the order of 100 km), a large antenna structure is required. Practical antennas of reasonable cost include either a horizontal wire strung on poles over the ground or temporary vertical wires supported by a balloon [*McPherson et al.*, 1974] or helicopter. However, such a vertical antenna does not provide year-round operation because weather and other factors severely restrict its periods of use. The ground-supported horizontal dipole, on the other hand, can be operated at any time. Ordinary ground is usually unsatisfactory as a base because its electrical losses are high at very low frequencies. What is needed is a thick (~2 km) low-loss material, such as an ice sheet, that will give antenna efficiencies of the order of 1% or better.

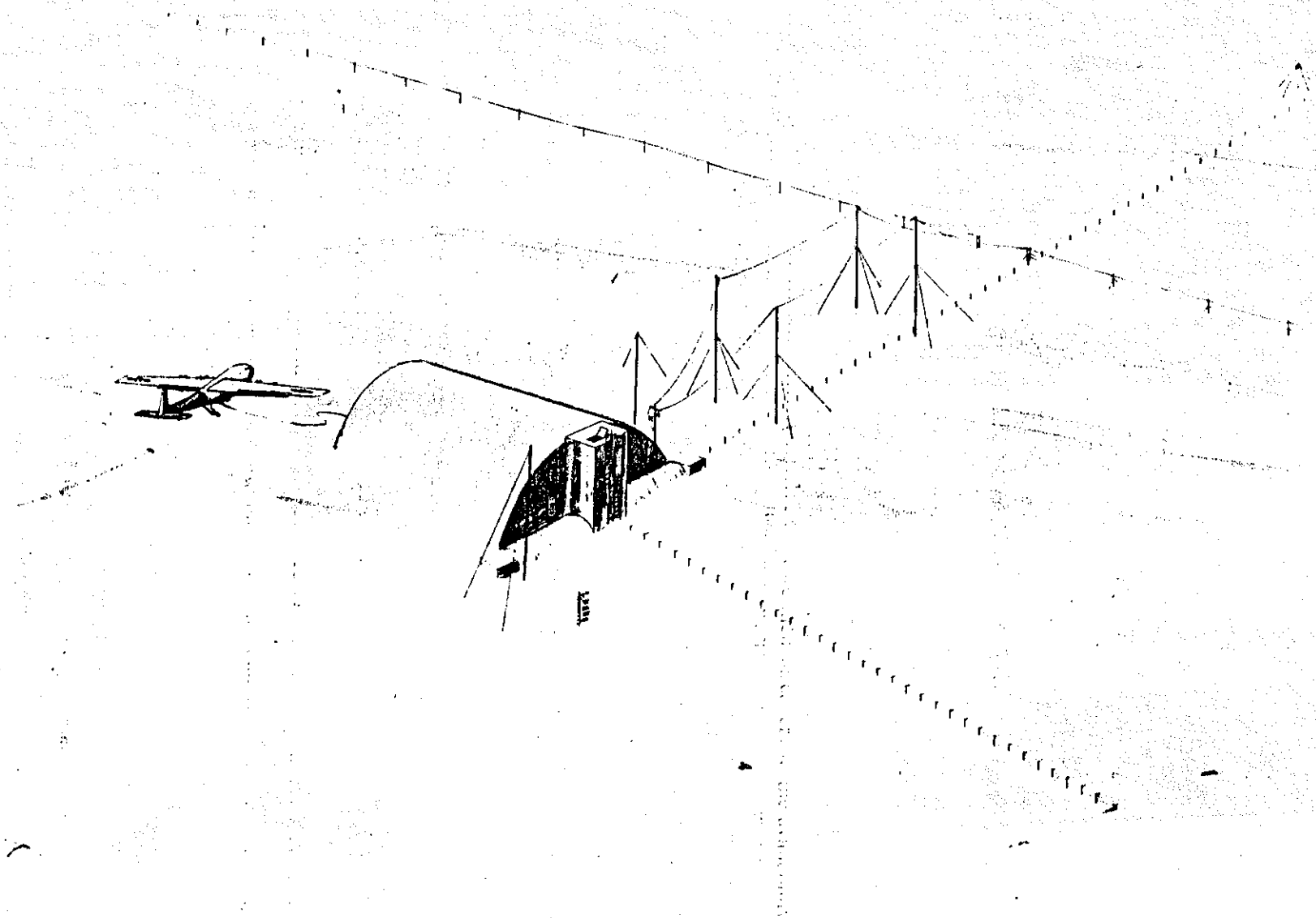

Plate 1.1. Conceptual view of Siple showing station being refueled (diesel) from ski-equipped C-130 Hercules aircarft. Passive experiment sensors are shown at upper and lower right. All other passive experiment sensors are located in vaults in the ice. Feedline to the 21.2-km antenna from station is carried on ~22-m towers. Other towers near the station are for communication and amateur V beam antennas.

W16

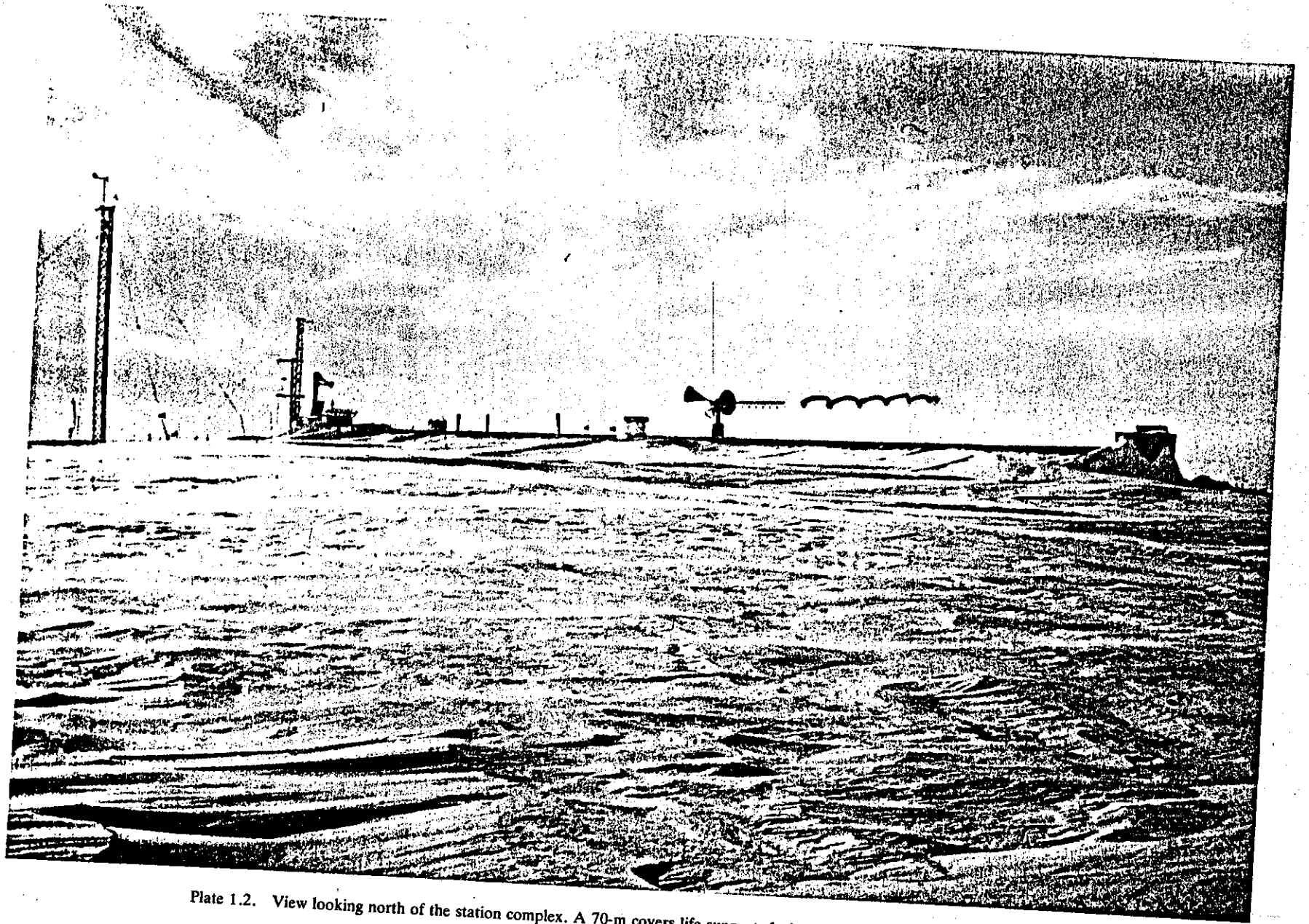

Plate 1.2. View looking north of the station complex. A 70-m covers life support, fuel, and science facilities. The photograph was taken in December 1973.

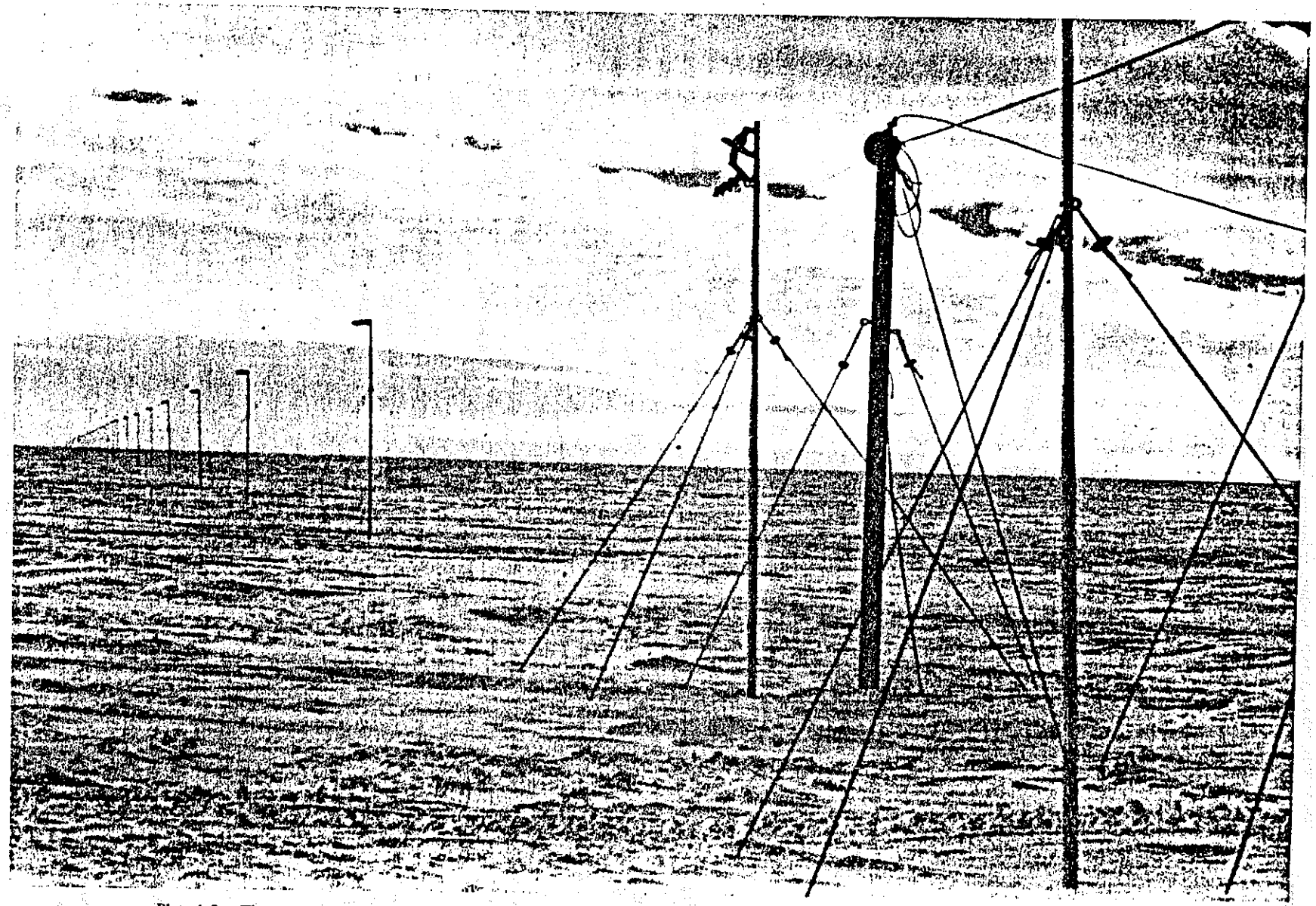

Plate 1.3. The east leg of the 21.2-km dipole antenna. The ice sheet is essentially flat over a 120-km distance in all directions from Siple.

The base of the Antarctic Peninsula appears to be the only location on the earth's surface that simultaneously satisfies the four conditions just stated. This region has other desirable characteristics including, for example, many lightning sources in the conjugate region. The whistlers excited by them provide information on the thermal plasma environment as well as on naturally occurring emission activity. Such information is needed to optimize the use of the transmitter and to analyze the results in terms of propagation path and resonant particle energy. Because thunderstorms are virtually absent in the Antarctic, the VLF noise level is unusually low, so that better signal-to-noise ratios can be obtained. Also, for reasons as yet unknown there appear to be more whistler ducts in the longitude sector of the Antarctic Peninsula than elsewhere in the world.

The purpose of the active wave experiments is to understand how VLF waves interact with energetic particles in the magnetosphere. The mechanism as currently understood is illustrated in the sketch of Figure 1.1. Signals from the transmitter enter a duct of enhanced ionization where they are trapped, just as light waves are trapped in an optical fiber. They are amplified, and emissions are triggered near the equatorial plane of the magnetosphere. These waves scatter energetic particles into the loss cone, causing a variety of disturbances in the ionosphere. Understanding this interaction is important because of the role played by the waves in diagnostics of the magnetosphere, their possible impact on VLF and ULF communications, and their control of radiation belt particles.

Taking a broader view, we expect that the interactions under study here will be present in a wide range of plasmas, both natural and man-made. As we shall see, the phenomena are complex and require controlled experimentation for their elucidation. Thus these magnetospheric experiments can be expected to aid in the understanding of plasma physics in general.

Several new results have been obtained by using the Siple transmitter and are briefly summarized here. More detailed discussion is given in section 4.

1. The output signal grows exponentially with time, usually at the frequency of the stimulating signal, at rates ranging from 25 to 250 dB/s. Total growth (ratio of output to input) varies typically from 20 to 35 dB. Since 30 dB corresponds to 3 orders of magnitude in signal power, magnetospheric amplification effectively raises the transmitter-radiated power from 1 kW to 1 MW.

2. Emissions are triggered either at or before the termination of the stimulating signal. Initial growth of emissions nearly always occurs above the frequency of the stimulating signal. The traces of emissions and signals on the frequency-time plane generally do not cross one another.

3. Siple transmitter experiments provided important clues that led to the finding that harmonic radiation from the North American power grid is

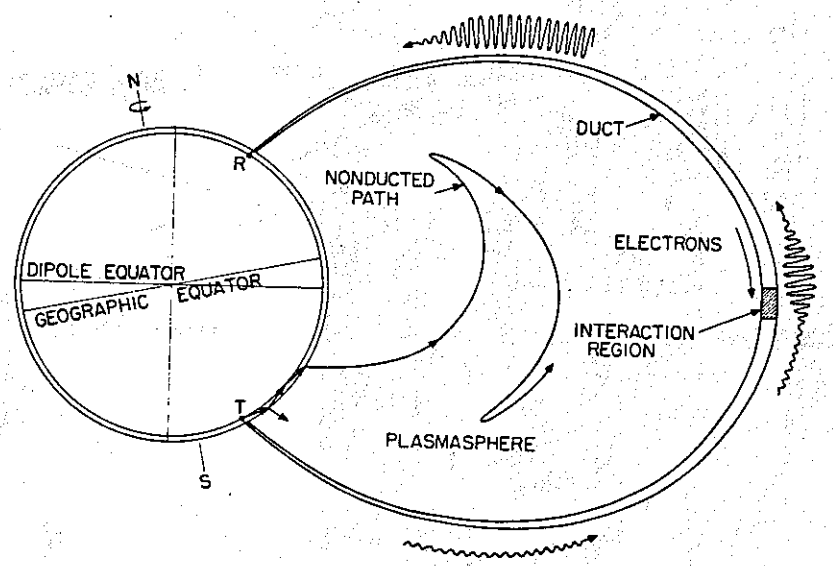

Fig. 1.1. Signals from T (transmitter) are both reflected and transmitted at the relatively sharp lower boundary of the ionosphere. Nonducted signals generally do not return to earth; they are observed on satellites. Ducted signals return to earth at R (receiver); they are amplified and trigger emissions near the equatorial plane.

frequently observed to trigger emissions and to interact with other magnetospheric signals.

4. Growth of coherent signals is suppressed by echoes of previous signals.

5. Free-running oscillations react strongly with externally injected waves when their frequency separation is less than about 50 Hz. Cutoff or total entrainment of the natural oscillation can occur even when the external signals are weaker by 20 dB or more.

6. Quiet bands (bands of reduced magnetospheric noise) can appear just below the amplified signal from the transmitter or from power lines. The width of the quiet band may vary from 50 to 200 Hz, and the level of quieting exceeds 6 dB. There is a delay of many seconds in the appearance and recovery of a quiet band with respect to the stimulating signal.

7. There is some evidence that ULF (~1 Hz) waves can be excited by Siple VLF transmissions [*Fraser-Smith and Cole*, 1975].

8. Satellites regularly observe both ducted and nonducted Siple signals and their associated emissions.

The results of the VLF wave injection experiments are interpreted in a preliminary way in terms of a phenomenological theory outlined in section 3. It should be kept in mind that there is as yet no complete theory describing the experimental results that are presented here. The theory is difficult because the interaction between the particles and waves is nonlinear. Most approaches to this problem have been based on linearized approximations to the fundamental equations of classical plasma physics. Such theories do not describe most of the observations. Thus the theorist faces a formidable challenge to develop theories that do.

2. BACKGROUND

Controlled wave injection experiments using a VLF transmitter were inspired by the fascinating natural phenomena of whistlers and VLF emissions, described in the preceding chapter. Whistler mode echoes from a VLF transmitter (NSS, 15.5 kHz) were first detected in 1957 [*Helliwell and Gehrels*, 1958]. Emissions stimulated by VLF transmitter signals (NPG, 18.6 kHz) were seen by chance on whistler tapes from New Zealand. Then an experiment conducted on the *Eltanin* off the Palmer Peninsula showed emissions triggered by signals from NAA (14.7 kHz) at Cutler, Maine [*Helliwell et al.*, 1964].

Because of the key role played in this work by the NAA observations, some of those results are shown in Figure 2.1. Most surprising was the fact that every Morse dash (150 ms) produced a strong emission, whereas the dots (50 ms) produced virtually none. At the same time the repeatability of triggering by dashes demonstrated that during favorable periods the plasma was always 'ready to fire,'

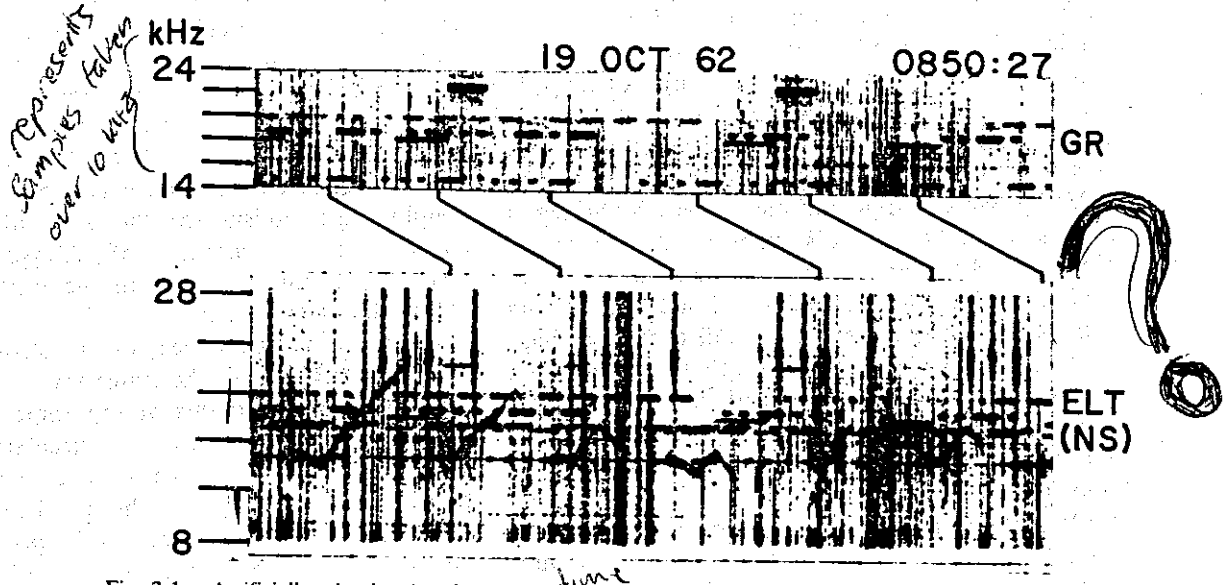

Fig. 2.1. Artificially stimulated emissions triggered by Morse code dashes from the U.S. Navy VLF transmitter, station NAA, located near Cutler, Maine. The upper spectrum shows code transmissions recorded at Greenbank, West Virginia. The lower spectrum shows the emissions observed on the research vessel *Eltanin* while on station just north of the Antarctic Peninsula. Inclined lines connect each transmitted dash with its corresponding emissions, observed 0.7 s later [*Helliwell*, 1965].

requiring only a suitable input wave to get the instability started. This experiment gave further support to the idea that emissions are triggered by wave packets rather than by the passage through an interaction region of a discrete bunch of energetic particles, as had been postulated earlier. More important, the NAA experiments demonstrated the feasibility of controlled VLF wave injection experiments.

Initial efforts to generate usable whistler mode waves from an antarctic transmitter were centered at Byrd Station (80°S, 120°W) in the auroral zone during the period 1966–1971. A long wire was laid on the ice and was excited at a number of different frequencies in the VLF band. As the snow cover increased, differential movement of the ice sheet caused frequent breaks in the wire, making regular operation impossible. Because of the high latitude and the low efficiency of the antenna, which was in direct contact with the ice, no whistler mode echoes were detected on the ground at either end of the magnetospheric path. However, the transmitter did provide new data on the properties of the auroral *D* region [*Helms et al.*, 1968]. In addition, an experiment on the effect of antenna polarization on the excitation of whistler mode signals was made with the aid of the Ogo 2 satellite [*Siren*, 1974]. With this experience as background and with new data on the plasmapause, obtained from whistlers recorded at Eights and Byrd, it was clear that the transmitter should be moved to a region near $L = 4$. By applying the criteria mentioned in section 1 the location of Siple Station was easily selected.

Additional interest in VLF wave injection experiments has been created by the observation of wave-induced particle precipitation. One such experiment was the stimulation of bremsstrahlung X rays (>30 keV) by whistler-triggered emissions [*Rosenberg et al.*, 1971]. Details of this experiment are given in chapter 3. Another was the perturbation of subionospheric VLF propagation associated with strong whistlers [*Helliwell et al.*, 1973], discussed in chapter 4. Both experiments showed that whistler mode waves could produce significant enhancements of electron concentration in the lower ionosphere.

Finally, there was the theoretical prediction that whistler mode waves should play a role in the control of the radiation belts [*Dungey*, 1963; *Cornwall*, 1964; *Kennel and Petschek*, 1966]. Both Dungey and Cornwall showed that whistlers could be expected to cause significant pitch angle diffusion of electrons through cyclotron resonance. Kennel and Petschek showed that the energetic plasma would tend to approach a condition of marginal stability in which wave growth was just sufficient to produce a wave intensity that would limit the particle flux by pitch angle diffusion. This theory meant that to understand the radiation belts, one must first understand the nature of the wave-particle interactions. Thus both theory and experiment suggested that controlled wave injection would indeed be a valuable new tool in magnetospheric research. These expectations have been amply realized.

As will be shown below, the experimental results require fundamental extensions to the theory of wave-particle interaction. The Kennel-Petschek theory is limited to broadband waves and does not explain the experimental results to be described in section 5. Thus we need new theory as well as more experimental data.

3. THEORY

Before we discuss current theoretical work on VLF wave-particle interactions, a general comment on energy exchange is in order. How do energetic charged particles exchange energy with VLF waves? The wave's electric field must do work on the particle. The principal mechanisms for this interaction are longitudinal and transverse resonance [*Brice*, 1964]. In longitudinal resonance (also called Cerenkov or traveling wave tube resonance) the parallel velocity of the particle equals the parallel component of the wave velocity. Then the parallel electric field of the wave as seen by the particle is constant. Thus depending on the position of the particle in the wave, this electric field can either accelerate (as in a linear accelerator) or decelerate (as in a traveling wave tube) the particle. Correspondingly, the wave is either attenuated or amplified. Longitudinal resonance is thought to be the coupling mechanism for the generation of VLF auroral hiss [*Jørgensen*, 1968; *Maggs*, 1976] but has not yet found a role in the generation of noise within the plasmasphere.

In transverse resonance, or cyclotron resonance as it is usually called, the transverse velocity of the spiraling particle rotates at the same rate as the transverse electric field of the circularly polarized wave as seen by the particle. It is this transverse field that does work on the particle. Cyclotron resonance is widely accepted as the principal mechanism for the generation of discrete VLF emissions and for the precipitation of energetic particles.

The phenomenon of cyclotron resonance can be understood as follows. The circularly polarized whistler mode wave is assumed to travel along the static

magnetic field. An energetic electron spirals around the earth's magnetic field as it bounces back and forth between its mirror points. Its motion parallel to the earth's field causes the wave frequency 'seen' by the electron to be Doppler-shifted either down or up depending on whether the wave is traveling parallel or antiparallel to the electron parallel velocity. The Doppler-shifted wave frequency f' depends on the wave frequency f, the wave number k, and the electron parallel velocity $v_\parallel$ and is given by

$$f' = f - (k/2\pi)v_\parallel \tag{3.1}$$

Whistler mode waves propagate only at frequencies below the gyrofrequency of the background plasma. Hence a nonrelativistic electron must travel opposite to the wave velocity to experience cyclotron resonance. This means that $v_\parallel$ is a negative number in (3.1). Cyclotron resonance occurs when the Doppler-shifted wave frequency f' equals the electron local gyrofrequency f_H and is therefore given by

$$f_H = f - (k/2\pi)v_\parallel \tag{3.2}$$

As was noted in section 2, classical wave-particle interaction theory is limited in its ability to account for the new observations. The basic nature of the problem is perhaps best illustrated by the long-enduring (many seconds) narrow band self-excited emission [*Brice*, 1964]. Because such emissions last much longer than the bounce time of the resonant particles, direct generation by bunches of energetic electrons satisfying (3.2) was ruled out. As an alternative, it was postulated that the natural oscillations resulted from feedback between the waves and cyclotron resonant electrons traveling in the opposite direction [*Brice*, 1963]. The coupling took place in an interaction region located near the equatorial plane. In this concept the magnetic field of the wave perturbed the relative longitudinal positions of the resonant electrons as they entered the interaction region, so that they formed a helical stream with the same pitch as the wave. These phase-bunched electrons then acted like circularly polarized antenna elements in an end-fire array. New electrons were constantly passing through the interaction region, each giving up a small fraction of its kinetic energy to the wave.

Later it was shown [*Helliwell*, 1967] that the inhomogeneity of the background plasma did in fact permit phase bunching to occur for reasonable wave magnetic field intensities (~1 mγ). Electrons could remain in resonance with a coherent wave train for several hundred wavelengths, an actual distance of the order of 1000 km. An extension of this analysis showed that the interaction length was independent of df/dt to first order [*Helliwell*, 1970]. This meant that growth and triggering would be qualitatively the same for signals of rising and falling frequency as for those of constant frequency.

To understand phase bunching, we consider only the primary interaction force, the full treatment being unnecessarily complicated for our purpose here. Consider a wave front that is normal to B_0, as shown in Figure 3.1*a*. Electrons flow into the paper at a pitch angle $\alpha = \tan^{-1}(v_\perp/v_\parallel)$ (see Figure 3.1*b*). They rotate in the left-handed (counterclockwise) sense so that they follow the helical paths described by the tips of the magnetic ($B_\perp$) and electric ($E_\perp$) field vectors of the whistler mode wave. (In Figure 3.1*a* the wave comes out of the paper, and its polarization is right-handed looking in the direction of propagation.)

Twelve helical streams of electrons, equally spaced in phase with respect to $B_\perp$, are shown in Figure 3.2*a* as they would appear before ($t = 0$) any phase bunching has occurred. Consider a representative electron whose $v_\perp$ makes an arbitrary initial angle ϕ with the local $B_\perp$ of the wave, as shown in Figure 3.1*a*. Applying the Lorentz force law, we see that the nonrelativistic longitudinal (along B_0) perturbation force is given simply by

$$F_\parallel = m\, dv_\parallel/dt = -|q|\, v_\perp B \sin\phi \tag{3.3}$$

where m is electron mass and $|q|$ is the magnitude of charge on the electron.

According to (3.3), which is the equation of a

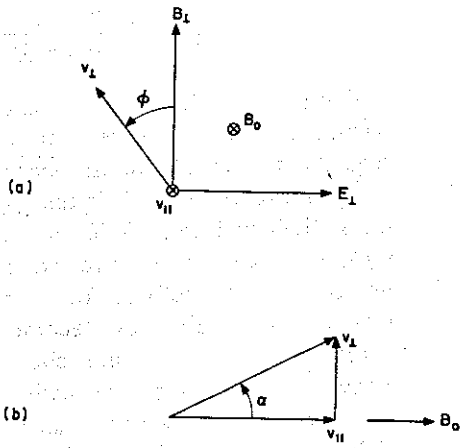

Fig. 3.1. (*a*) Relation between wave fields $E_\perp$ and $B_\perp$ and electron velocity components $v_\perp$ and $v_\parallel$. Earth's field is denoted by B_0, and phase angle by ϕ. (*b*) Relation between electron velocity v and B_0. Pitch angle is denoted by α.

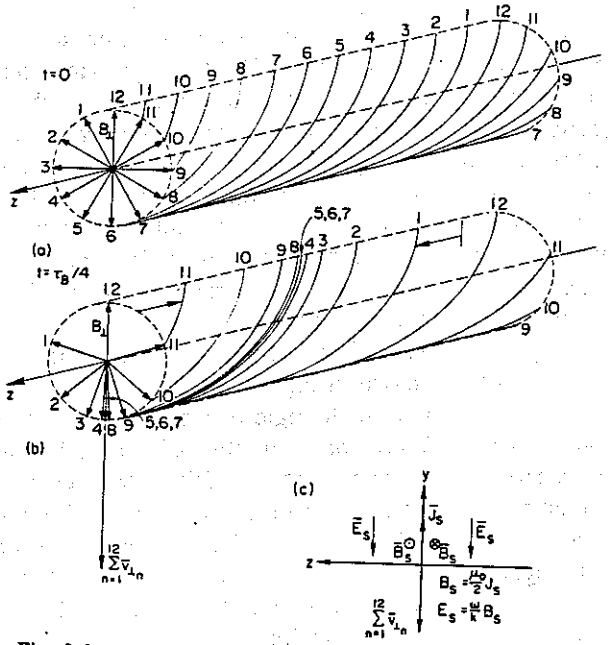

Fig. 3.2. (*a*) Helical loci of the perpendicular velocities of 12 elementary electron streams before bunching ($B_\perp$ is represented by vector 12). (*b*) Same loci after some bunching has occurred. (*c*) Effective sheet current J_s and associated stimulated magnetic (B_s) and electric (E_s) fields [after *Helliwell and Crystal*, 1973, Figure 3].

simple pendulum, each electron is displaced toward a position where $\phi = \pi$, called the stable point. The time required for an electron to reach the stable point for the first time is one quarter of the pendulum period (also the reciprocal of the 'trapping' frequency f_T) and is called the bunching time, τ_B. For small initial values of $(\pi - \phi)$ the bunching time is a constant and is given by

$$\tau_B = \left(\frac{\pi^2}{4}\frac{m}{q}\frac{1}{kv_\perp B_\perp}\right)^{1/2} \tag{3.4}$$

The remarkable result of this process is that for a particular guiding center, all resonant electrons, regardless of their initial phase, tend to line up along the same helix. This tendency is illustrated by the helices of Figure 3.2*b*, which is drawn for $t = \tau_B/4$. Here all helices have moved toward the position occupied by helix 6. For example, the respective relative longitudinal displacements of the helices numbered 1 and 11 are shown by longitudinal arrows. At any transverse section the vector sum of the transverse velocities $\sum_{n=1}^{12} \bar{v}_{\perp n}$, properly normalized and multiplied by the charge density, gives the transverse current density. In any selected stream segment this distributed current can be represented by a current sheet $J_s A/m$ obtained by multiplying the current density by the segment length. Each such current sheet can be visualized as a source of stimulated wave fields B_s and E_s, as shown in Figure 3.2*c*. Only those stimulated wavelets traveling to the left add coherently to form a net stimulated signal. This stimulated signal may remain at the frequency of the triggering signal, or it may change frequency, in which case it is called a 'triggered emission.' To obtain a quantitative solution to this problem, it is necessary to consider the time and space variations of both the bunching field $B_\perp$ and the resulting stimulated current. However, a complete self-consistent solution to this problem has not yet been obtained. Computer simulations have been employed to obtain some approximate descriptions of the mechanism [*Helliwell and Crystal*, 1973; *Nunn*, 1974].

An important factor in coherent wave growth is the bandwidth of the signal. From our discussion it is clear that for effective phase bunching the driving field must remain essentially coherent for one bunching period. Thus any modulation of the wave must be confined to a band less than roughly $\pm\Delta f$, where $\Delta f = 1/\tau_B$. For a bunching time of 30 ms, $\Delta f \simeq 33$ Hz. On the other hand, it is also clear that interfering signals well outside this band will have relatively little effect on the growth, unless they are much stronger. As wave intensity increases, τ_B becomes smaller, as is shown by (3.4), so that the τ_B of the interfering signal must be comparable to the reciprocal of the frequency separation for significant interference to occur.

Interaction between VLF waves and electrons is not the only application of cyclotron resonance in the magnetosphere. As *Brice* [1964] has shown, ULF (~1 Hz) waves and protons interact in a similar way. Thus we may not be surprised to find many VLF phenomena repeated at ULF.

An important aspect of wave-particle interaction is the precipitation of resonant electrons. When we assume a wave function, it is a straightforward task to calculate approximately the perturbations in the orbits of representative test particles, beginning with (3.3). In general, cyclotron resonance wave growth is accompanied by a decrease in the pitch angle [*Brice*, 1964]. Electrons near the loss cone can then be dumped into the ionosphere, where they convert their considerable kinetic energy (many keV) into other forms (e.g., ionization, light, X rays, and heat). The kinetic power carried by this precipitation flux may be as much as 6 orders of magnitude higher than that of the input triggering wave. A simplified analysis based on cyclotron resonance shows that coherent waves of the order of 10-my

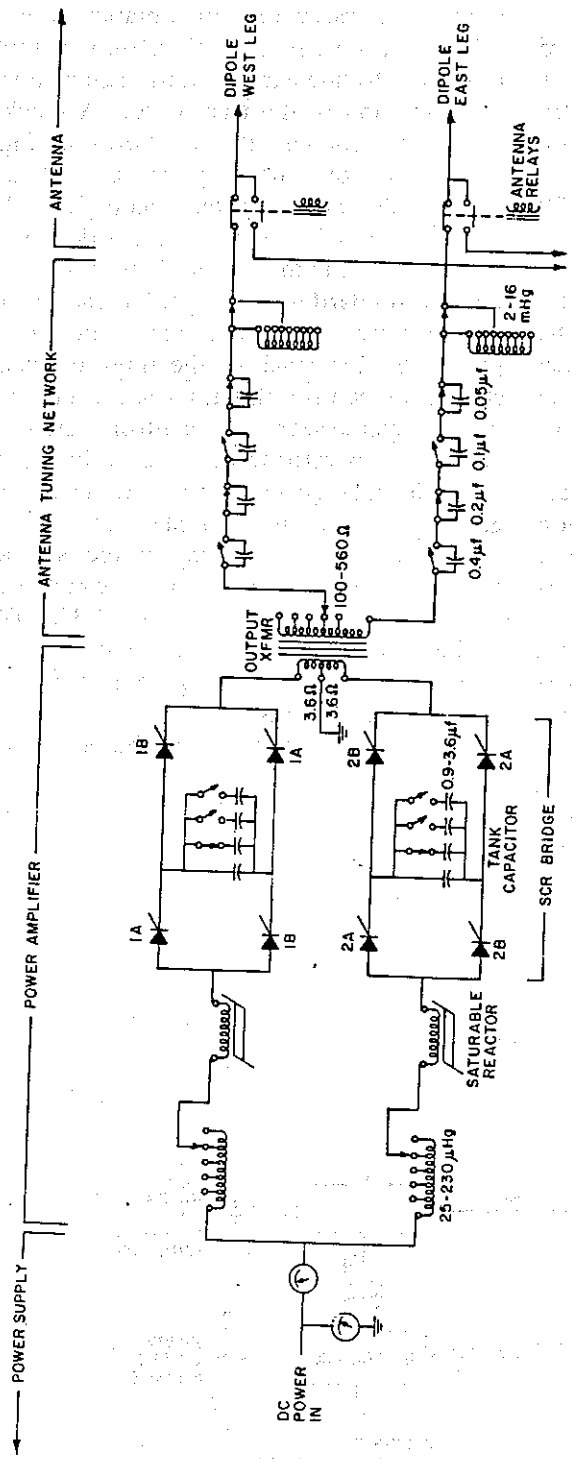

Fig. 4.4. Transmitter diagram of the VLF transmitter power supply, power amplifier, and antenna tuning network.

the transmitter signals as well as other man-made and naturally occurring signals.

The transmitter selected for this role was a surplus unit provided on loan by the Office of Naval Research of the U.S. Navy. Figure 4.1 shows a block diagram of the transmitter system, consisting of three basic parts: (1) the antenna and matching network, (2) the power amplifier, and (3) the control system.

4.1. *Antenna*

Analysis of the electrical characteristics of the Siple Station site [*Raghuram et al.*, 1974] showed that a long horizontal dipole erected at least 5 m above the ice would provide an efficiency of about 2% at a frequency of 6 kHz. Thus with an effective input power from the transmitter of, say, 50 kW it would be possible to radiate 1 kW upward into the magnetosphere at a frequency of 6 kHz.

The actual antenna is a 21.2-km horizontal dipole supported above the snow surface and aligned with the local magnetic east-west direction. The antenna conductor is made of number 2 AWG stranded (7) aluminum wire supported on 350 ~5 cm x 13 cm x 6 m aluminum channels placed in the snow about every 60 m. The wire is insulated from the supports by high-voltage (60 kV) porcelain insulators.

The resonant frequency of the antenna lies between 4.8 and 5.2 kHz, depending on the height above the snow. The antenna was designed to resonate at 5 kHz. Figure 4.2 shows the impedance of the antenna versus frequency, as measured in June 1973, when the antenna was an average of 1.5 m above the snow surface and again in January 1974, after it had been raised to 4.6 m above the surface. The effects of proximity to the snow surface are (1) to reduce the antenna phase velocity, thus lowering the resonant frequency, and (2) to increase the losses, thus reducing the Q of the antenna.

The efficiency of the antenna decreases as it approaches the snow, because the losses arise primarily from currents induced in the volume of snow close to the antenna wire. Thus it is necessary to keep the antenna at least several meters above the surface, rather than lay the wire on the surface as was done at Byrd Station. The calculated antenna radiation efficiency versus frequency is shown in Figure 4.3 for a height of 5 m. Although antenna efficiency drops off rapidly at lower frequencies, stimulated emissions have been observed as low as 1.9 kHz.

4.2. *Transmitter*

The transmitter power amplifier is the heart of the wave injection system (see Figure 4.4 and Plate 4.1). It amplifies signals from the control circuitry and delivers them to the antenna. The amplifier is a fairly compact solid state unit of high efficiency, generating a maximum power output of over 100 kW from 5 to 20 kHz. It can be used at frequencies as low as 1.5 kHz.

The amplifier uses silicon controlled rectifiers (SCR's) to switch currents through tuned circuits, producing a series of half-sine wave pulses which are combined in the output transformer to form the sine wave output. The tuning of the transmitter determines the duration of the half-sine wave pulses, and signals from the control circuitry determine the starting times of these pulses. In addition to the tuned circuits in the transmitter there is a matching network used to reduce the reactive voltages at the antenna to safe limits for the transmitter. A tapped output transformer, covering impedances between 100 and 590 Ω, matches the resistive part of the antenna impedance at different frequencies (see Figure 4.4). The power amplifier losses are relatively small, giving an overall efficiency for the transmitter system of approximately 80%.

The transmitter control circuits determine the times and frequencies of transmissions and monitor the operation of the transmitter. A block diagram of the control circuitry is shown in Figure 4.5. Central to the control system is a Data General Nova 1220 minicomputer (Plate 4.2). This computer receives 10-ms clock pulses derived from the station's rubidium standard (quartz crystal frequency standard for backup). Its real time operating system works in 10-ms frames, counting the clock pulses to keep track of the time and sending out signals to control the transmitter keyer and frequency synthesizer. The control system computer allows the operator to write transmitter programs in a high-level language which makes complicated programs relatively easy to implement.

The actual frequency transmitted is generated by a direct frequency synthesizer, which can be remotely controlled in steps of 0.01 Hz. The output of the synthesizer and the transmitter key signal are sent to the exciter, which generates the gate pulses for the transmitter SCR's.

The monitor system allows the operator to watch

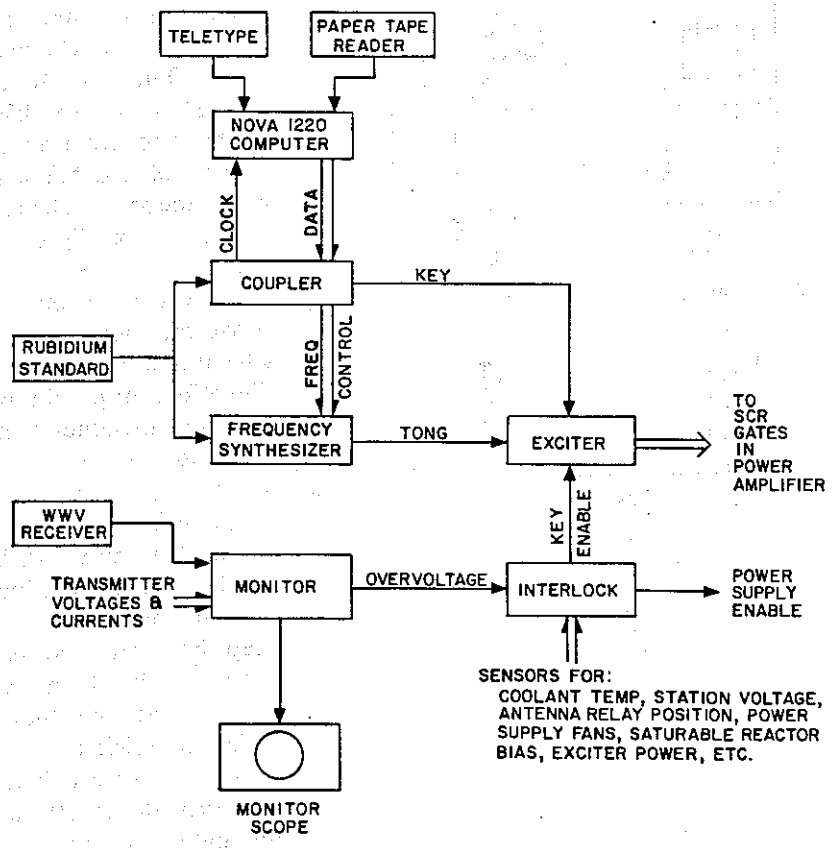

Fig. 4.5. Transmitter control system diagram. The circuits control times and frequencies of transmissions and also monitor the operation of the transmitter.

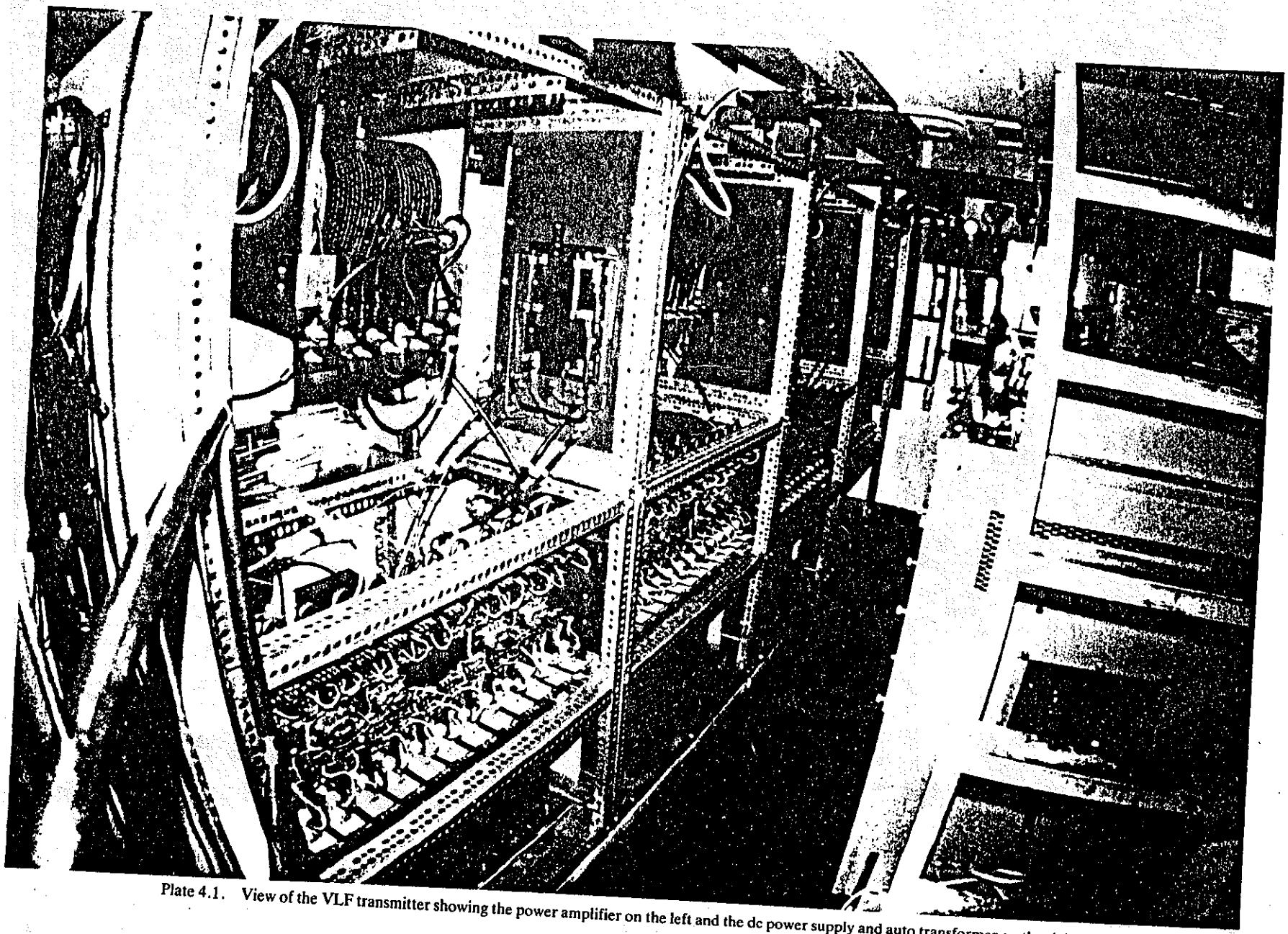

Plate 4.1. View of the VLF transmitter showing the power amplifier on the left and the dc power supply and auto transformer on the right.

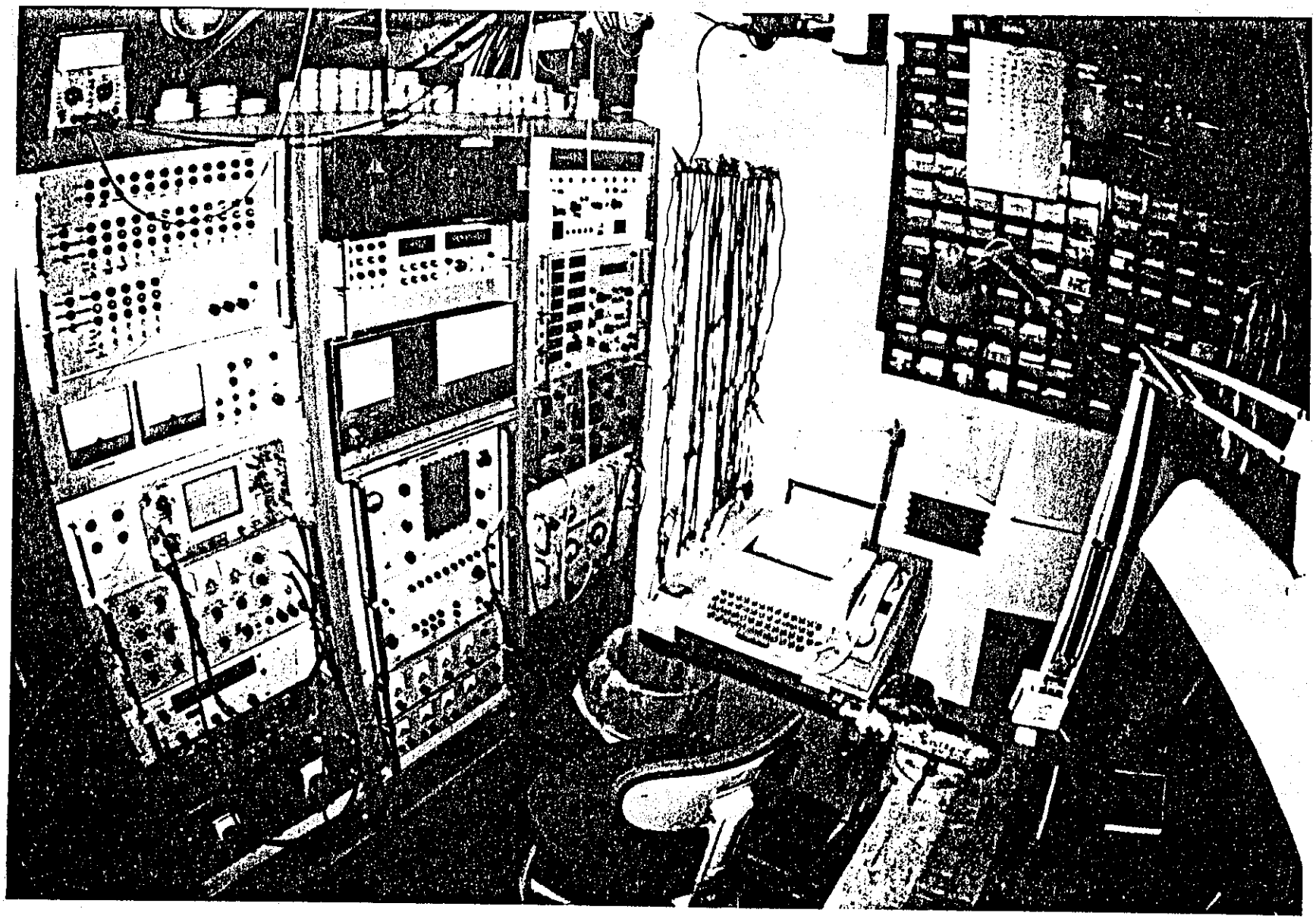

Plate 4.2. View of the transmitter control modules. A Data General Nova 1200 minicomputer is the central instrumentation of the control system.

various current and voltage wave forms in the transmitter. The interlock system monitors various parameters of the transmitter, such as antenna and tank voltages, cooling system temperature, and station power level, and shuts the transmitter off in case of a fault.

The many automatic features of the transmitter instrumentation allow the operator to observe the natural VLF activity (for example, whistlers, whistler-triggered VLF emissions, periodic VLF emissions) between transmission intervals and adjust the transmitter frequency in order to optimize the stimulated wave-particle interactions. Best results are obtained when the Siple transmitter is tuned to the frequency where natural emissions are occurring. A real time spectrum analyzer (Rayspan) is used for the purpose of monitoring natural VLF activity as well as two-hop echoes of Siple transmissions.

VLF transmissions from Siple Station have averaged about 6 hours/day over the years 1973–1975. This year-round operational capability was to a great degree responsible for the success of the wave injection experiment.

4.3. *Receiving Systems*

We now review briefly the VLF receiving and recording facilities located at Siple and Roberval, Quebec, Canada (48°N, 73°W). A block diagram of the receiving system is shown in Figure 4.6. The signals are picked up by crossed loop antennas, which are sensitive to the magnetic field component of the incident wave. Balanced input circuits are employed to reduce system response to local electric fields. The receiving loops at Siple are larger in area than those at Roberval by a ratio of 5:1. This increased size actually improves the signal-to-noise ratio at Siple, since the background atmospheric noise level in the Antarctic is unusually low.

The loops and preamplifiers are located some distance away from the station so as to reduce interference from the power lines (Roberval) or from the station complex (Siple). At Roberval it is difficult to find a site free of interference for two reasons: (1) the power distribution system in the Province of Quebec employs local grounding (at transformers and other components) instead of carrying the ground wire throughout the power network; and (2) the bauxite reduction plants of the Aluminum Company of Canada, located approximately 80 km east of Roberval, generate considerable interference. A much quieter site for possible future use has been found in the Provincial Forest Reserve west of Roberval. The required electronic systems would be powered by batteries or by other power generation units (such as radioactive thermal generators).

The Siple VLF receivers have a flat frequency response from 220 Hz to almost 100 kHz. The lower cutoff of the Roberval receiver is set at 2 kHz to control interference from the local power line.

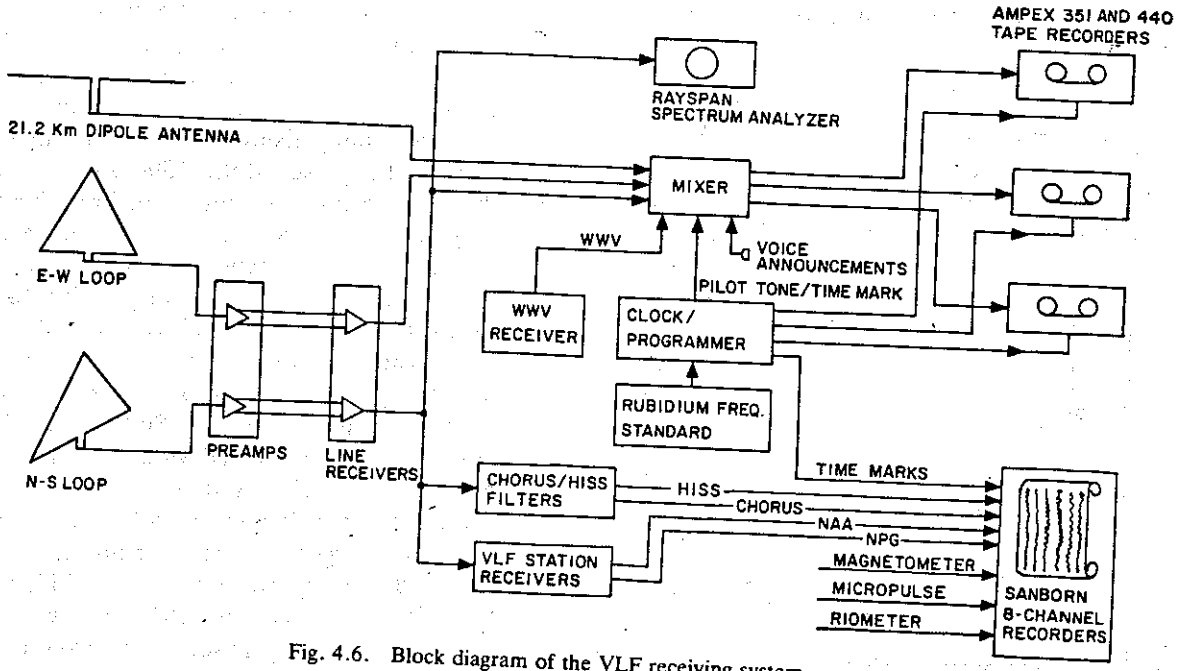

Fig. 4.6. Block diagram of the VLF receiving system.

The dynamic range at the outputs of the receivers at both stations is about 105 dB over a 30-kHz bandwidth. This wide dynamic range is necessary to prevent modulation between different signals in the received spectrum, especially between strong signals from certain VLF transmitters. Because of the limited dynamic range of the tape recorders (about 50–60 dB), however, it has been necessary to put notch filters in the Roberval receivers at 17.8 and 21.4 kHz to eliminate intermodulation products from the U.S. Navy VLF transmitters NAA (Cutler, Maine) and NSS (Annapolis, Maryland), respectively. The frequency response curves for the Siple and Roberval receivers are shown in Figure 4.7.

Broadband signals from the VLF receivers are recorded on standard 1/4-inch magnetic tape. A continuous pilot tone at 9 kHz is recorded along with the VLF signals. The pilot tone is detected by the analysis equipment and is used to compensate for tape speed variations. The pilot tone is also amplitude modulated (6–10 dB) to provide time marks on the second and station identification and time of day information in Morse code every minute. The time marks are generated by the system digital clock and are accurate to within 2 or 3 ms. In addition, WWV time announcements are recorded every 5 min.

It is necessary to have accurate timing information for use in the correlation of VLF events received at different stations and on satellites and for accurate measurement of the time delays between the VLF signals transmitted from Siple and received at Roberval.

5. EXPERIMENTAL RESULTS

The first three seasons (1973–1975) of operation of the Siple transmitter were mainly exploratory. The object was to optimize the parameters of the experiments and to identify and interpret new phenomena. The results have been most gratifying, the quantity of interesting data far exceeding expectations. Most runs have been examined, and those containing useful data have been spectrum analyzed. Selected phenomena have been interpreted in a preliminary way. The purpose of this section is to summarize the results obtained so far.

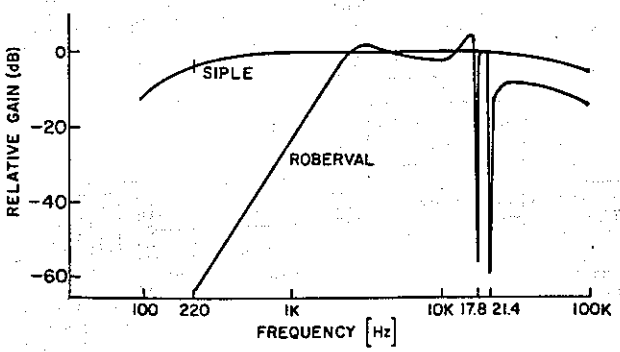

Fig. 4.7. Frequency response curves of the Siple and Roberval VLF receiving systems.

5.1. *Wave Growth and Emissions*

The first experiment using the Siple transmitter was aimed specifically at understanding the dot-dash anomaly described in section 2. A series of pulses of progressively increasing length was transmitted alternately on two frequencies, 5.0 and 5.5 kHz. The pulse lengths varied from 50 to 400 ms in steps of 50 ms. Five pulses were transmitted at each pulse length, so that the total sequence lasted 18 s, as is shown in Figure 5.1. The dynamic spectrum of the received pulses and their associated triggered emissions is shown in the lower panel. The signal amplitude in a 130-Hz band centered on 5.5 kHz is plotted on a logarithmic scale in the upper panel. Between the panels is shown the pulse length.

As the figure shows, the shorter pulses are relatively weak and trigger only falling tones. As the pulse length increases, the peak intensities of the pulses and their associated emissions increase. Measurements show that each pulse grows exponentially with time at the same rate (128 dB/s) until it either terminates or reaches the saturation level. As the pulse length and peak amplitude increase, there is a change in the character of the emissions. The shorter pulses produce mainly falling tones that begin at the end of the pulse, while the longer pulses ($\geq$300 ms) produce mainly rising tones that begin before the end of the pulse. Both 150- and 200-ms pulses show falling tones at pulse end. The whistler occurring at 8 s in Figure 5.1 is seen to be associated directly with a reduction (by a factor of 2) in the peak amplitude of the corresponding Siple pulse. This effect may be related to echo-induced growth suppression, discussed later. In addition, some of the stronger rising emissions appear to quench the growth of the succeeding Siple pulse. The latter effect may be connected with the quiet band phenomenon, also discussed later.

At the lower frequency (5.0 kHz) there is little growth or triggering. (At other times, a few minutes removed, activity was higher at 5.0 kHz than at 5.5 kHz [*Stiles and Helliwell*, 1977].) However, there is one medium-strength falling tone from the end of a 350-ms pulse. Thus the triggering behavior of a

long pulse having a low growth rate is similar to that of a short pulse with a large growth rate [*Stiles and Helliwell*, 1977].

The record of Figure 5.1 provides a natural explanation for the dot-dash anomaly observed in earlier experiments. For pulse lengths of 50 ms the output signal and its emissions, if any, are undetectable. When the pulse length reaches 150 ms, both the signal and its emissions appear above the background noise. It is found that the amplitude of the triggered emissions is about the same as that of the triggering signal just before triggering occurs. This explains why most dots do not trigger significant emissions; they do not last long enough to grow above the noise level.

The growth of coherent signals is further illustrated by the detailed behavior of a single 1-s pulse, shown in Figure 5.2 [*Stiles and Helliwell*, 1977]. The upper curve shows the frequency of maximum signal intensity obtained from a fast Fourier transform of a digital conversion of the original recorded data. The middle panel shows the amplitude of the peak component. Clear evidence of exponential growth appears between 0.25 s and 0.9 s, after which the amplitude is constant until the end of the pulse at 1.0 s. An emission is generated at the end of the pulse, as shown by the upper panel. (Because of multipath propagation there are signal components extending beyond 1.4 s.) The bandwidths of the signal and its associated emissions are shown in the lower panel. It is seen that the minimum bandwidth is 27 Hz, close to the bandwidth of an ideal monochromatic pulse as measured by using the same analysis technique [*Stiles and Helliwell*, 1975]. It is concluded that in this case the magnetospheric signal is essentially monochromatic up to the time of emission triggering [*Stiles and Helliwell*, 1977].

An important conclusion from records of this type is that the frequency of the exponentially growing signal is the same (within 1 or 2 Hz) as that of the input signal. After saturation occurs, the frequency of the received signal may change, but in such cases the initial direction of change is nearly always positive. The frequency may then either rise further or fall. Thus we have a phenomenon resembling a laboratory phase-locked oscillator in which the input and output frequencies are the same until a critical amplitude level is reached; then the free-running oscillation, or emission, begins. However, there are exceptions to this rule. Some pulses show more or less periodic fluctuations in frequency and amplitude during the growth phase, with periods of the order of 0.1–0.2 s. Emissions may also show periodic modulation. This phenomenon is not fully understood; it could be an instability in the feedback loop, synchronized in some cases by external signals such as power line radiation.

The relationship between growth rate and fre-

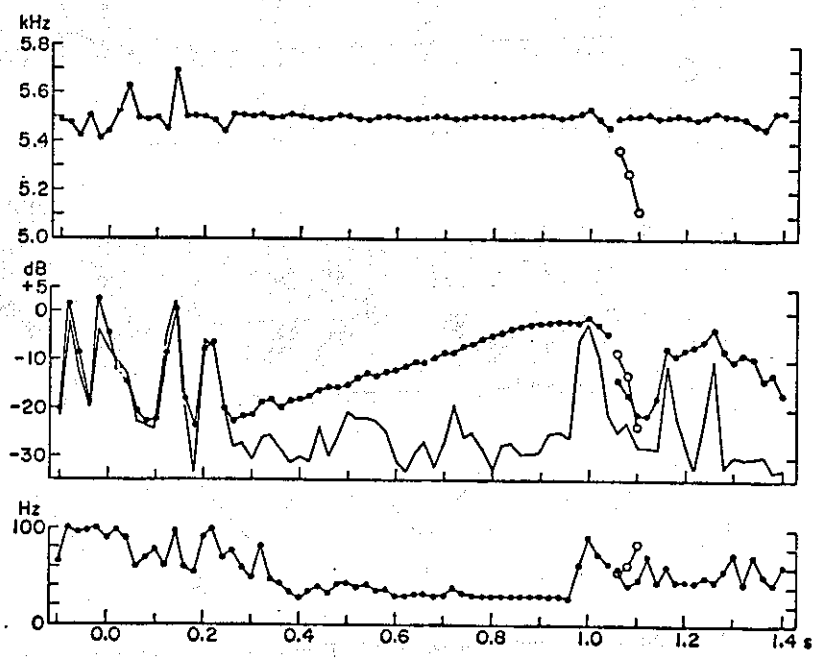

Fig. 5.2. Frequency, amplitude, and bandwidth of a 1-s pulse and associated emission. Open circles correspond to the second peak in the Fourier transform. The solid line in the amplitude plot measures power in a 1·75-Hz band that is close to, but does not contain, the signal.

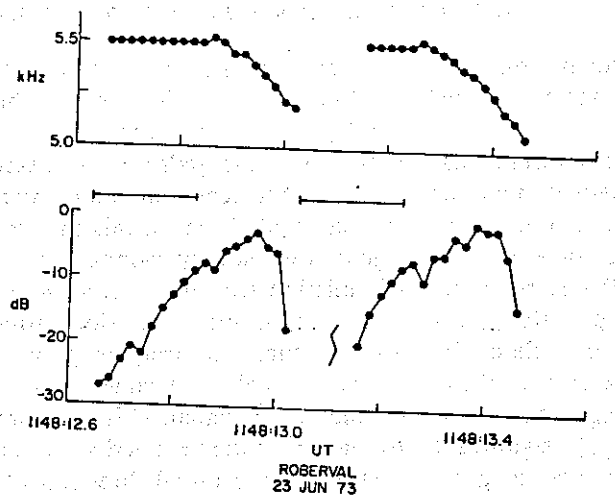

Fig. 5.3. Frequency and amplitude of emissions triggered by two 200-ms Siple pulses at 1148:12.6 UT, June 23, 1973. The horizontal bars denote the duration of the triggering signals [from *Stiles*, 1974].

quency change is critical in the development quantitative interaction models. To illustrate t relationship, the spectra of two 200-ms pulses a their associated emissions are shown in Figure 5. In both pulses the input signal terminates befc the intensity has reached its saturation level. At t end of the pulse there is a slight momentary redu tion in amplitude, and then the growth continu for another 6 dB or so, while the new frequenci are being generated. It is seen that the intensity a the rate of change of frequency with time va independently of one another, as predicted by *He liwell* [1967, 1970].

The role of *df/dt* in growth and triggering ca also be studied by using a frequency ramp progran illustrated in Figure 5.4. The transmission format shown in the lower panel, with the timing adjuste so that the transmitted signal coincides with th received signal on the main path. An importar

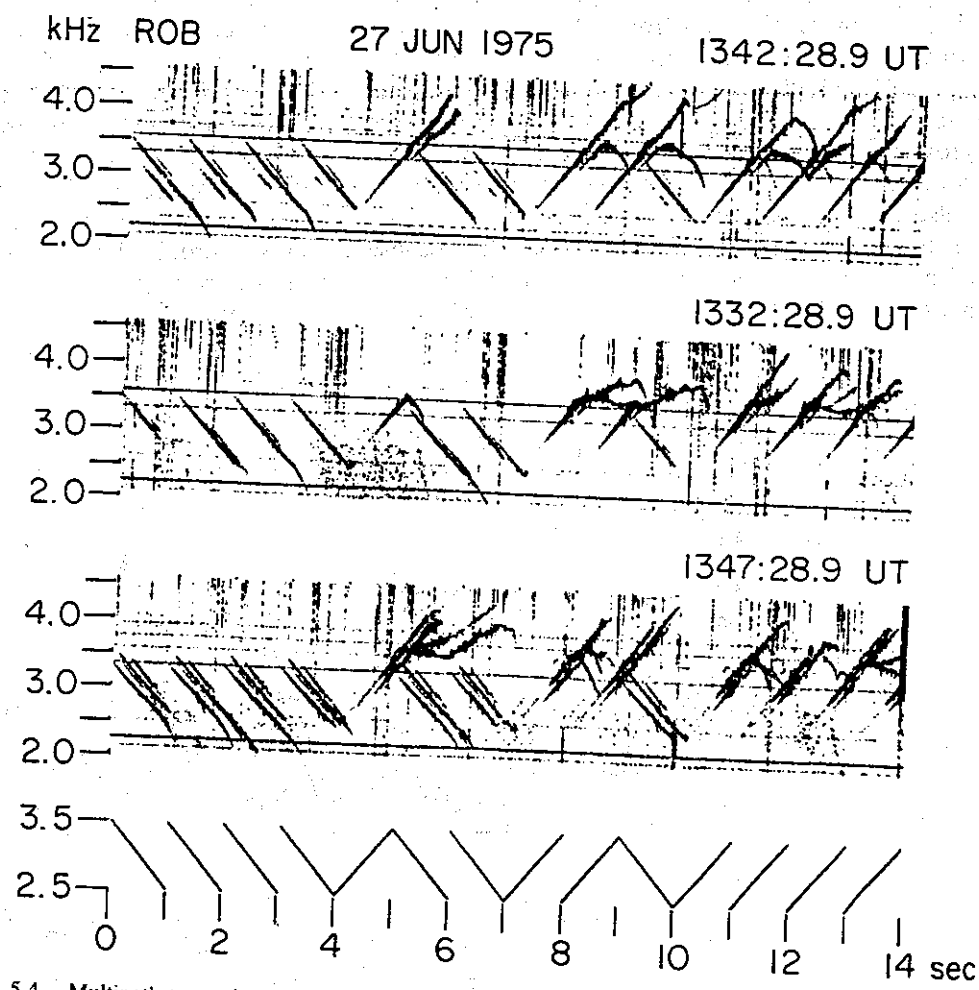

Fig. 5.4. Multipath transmitter signals and VLF emissions received at Roberval. Notice that the slope of many of the triggered risers is approximately the same as that of the transmitted signal. The maximum frequency of the transmitter signal is 3.5 kHz, whereas the maximum frequency of the emission is approximately 4.5 kHz.

advantage of the ramp is its ability to separate multipath signals. For example, in the lower part of Figure 5.4, each falling ramp is seen on three distinct paths, each path showing a different variation of amplitude with frequency, $A(f)$. Falling and rising ramps on the same path show different $A(f)$ behavior. The main reason is that the time required for growth causes the peak intensity to be reached toward the end of the pulse, so that the rising ramp is strong near 3.5 kHz and the falling ramp near 2.5 kHz.

The artificially stimulated emissions triggered by the strongest rising ramps in Figure 5.4 are frequently seen to have about the same slope as the ramps themselves. On other parts of the same run, risers triggered by constant frequency pulses show asymptotic slopes that are comparable to the ramp slopes (1 kHz/s). In general, the asymptotic slopes of triggered emissions are not sensitive to the slope of the triggering signal. At comparable frequencies the growth rates and total growth are about the same for rising and falling ramps as for constant frequency pulses. Growth is affected more by the value of frequency than by its time rate of change.

5.2. *Power Line Radiation*

Before continuing with the results of the Siple transmitter experiments, we shall describe another type of artificial wave input into the magnetosphere. In the course of the Siple experiments it was found that the triggered emissions often showed perturbations at some of the frequencies of the Roberval power system induction lines. This result suggested that the Canadian power grid might be radiating signals into the magnetosphere at harmonics of 60 Hz. Accordingly, a test was performed, using available data, for the coincidence of power line radiation (PLR) at Roberval and Siple Station [*Helliwell et al.*, 1975].

An example of the results is shown in Figure 5.5. The broad horizontal lines on the spectra are spaced roughly 120 Hz apart and are closely associated with the relatively thin induction lines shown on the spectrum from Roberval. (Some of these induction lines are identified on the right-hand side by their harmonic order.) The small separation between the magnetospheric lines and the induction lines is thought to result from the triggering of rising emissions by the actual power line harmonic component. These emissions form a somewhat irregular band just above the induction power line. What is clear from the conjugate records is the essential similarity between the two sets of magnetospheric lines. There is one important difference, however. Each line shows periodic intensity modulation which is in antiphase at the two ends of the path. Analysis

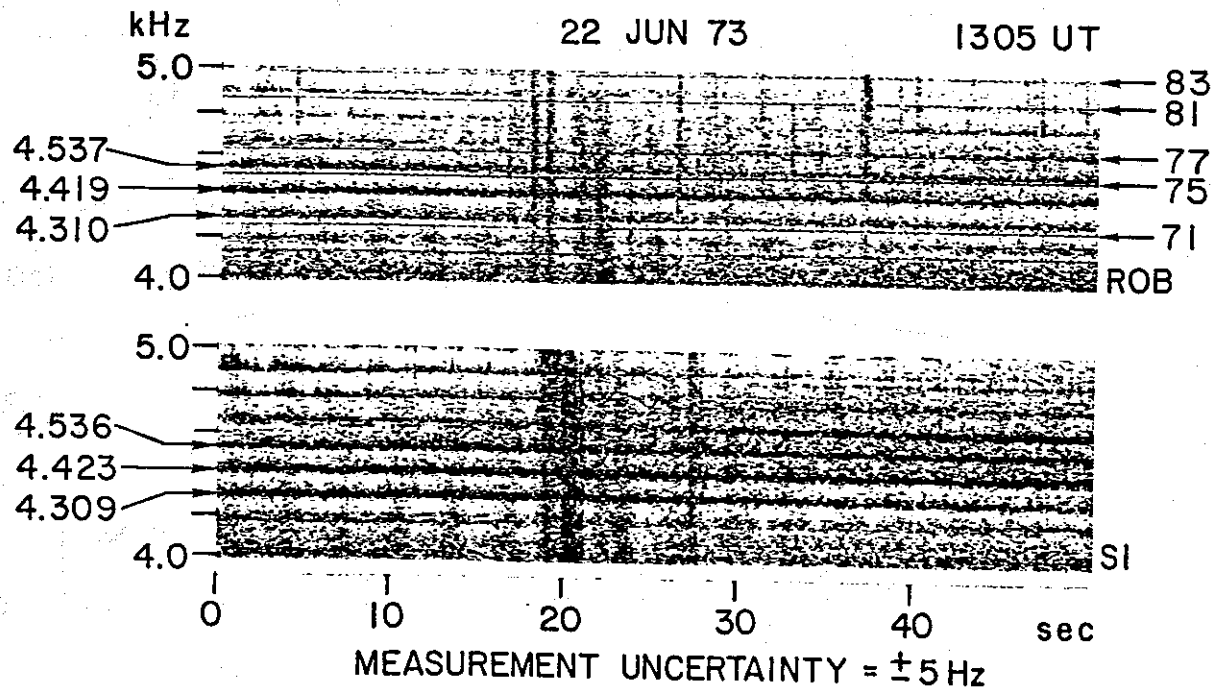

Fig. 5.5. Simultaneous spectra from the conjugate stations Siple and Roberval. The frequencies of prominent magnetospheric lines and the harmonic numbers of the induction lines seen at Roberval are given. Note the difference in bandwidth between magnetospheric and induction lines.

shows that the period is the same as the two-hop whistler period at the same frequency, thus confirming their magnetospheric origin. (The nearly vertical bands on Figure 5.5 are echoing whistlers.) Closely spaced self-generating lines of this type may possibly account for the so-called mid-latitude hiss, often seen at times of strong whistler echoing [*Helliwell et al.*, 1975].

Harmonic radiation from most power systems is highly coherent. Does it therefore produce coherent growth and triggering in the magnetosphere in a manner similar to radiation from a VLF transmitter? An example of transmitterlike behavior by PLR is shown in Figure 5.6. In Figure 5.6 (top), several multipath whistlers excite trains of echoes that gradually develop horizontal striations at fixed frequencies, presumably controlled by PLR. (Their spacings are typically 120 Hz.) With the passage of time, each line becomes narrower as the echoes of adjacent frequency components fade away. As the spectral lines become narrower, they behave more independently of one another and thus acquire the properties of isolated coherent signals. The details of this process are illustrated in Figure 5.6 (bottom), which is an expansion in time of a portion of the upper panel. The third echo group is relatively strong and pure and triggers strong fallers. This event closely resembles a ½-s-long Siple pulse and in isola might easily be mistaken for a VLF transmitter sig

Power line radiation can thus be expected control the magnetosphere in the same way as signals from the Siple transmitter. It will theref play an important role in future wave-particle exp iments on the magnetosphere.

5.3. *Growth Suppression*

We have seen how coherent signals can be am fied up to 20 or 35 dB during a passage through wave-particle interaction region in the magne sphere. Now we look at the complementary p nomenon of growth suppression [*Raghuram et* 1977*b*]. An example is shown in Figure 5.7. In t lower panel is a portion of the dynamic spectrum a single 30-s-long pulse from the Siple transmit on 5.15 kHz. In the initial 4 s the signal is ve strong and shows many triggered emissions. Afte s both signal strength and emission activity decre abruptly.

A quantitative measure of suppression is sho in the middle panel, where the square of the avera amplitude of 17 pulses is plotted versus time. O of these pulses is shown in the lower panel. T signal initially grows rapidly to an amplitude b tween 1.5 and 2.0 on the relative scale. After abo

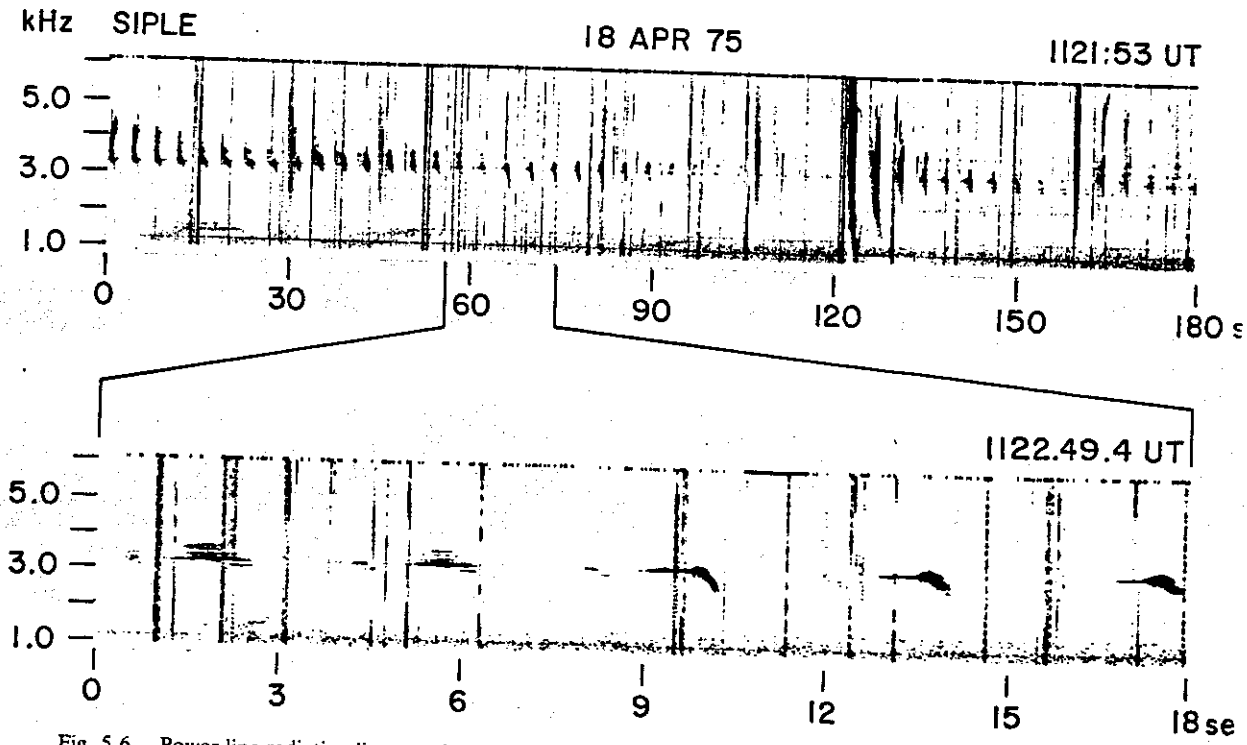

Fig. 5.6. Power line radiation lines on the lower panel have the appearance of pulses transmitted by VLF transmitters. The Siple transmitter was not on the air at this time.

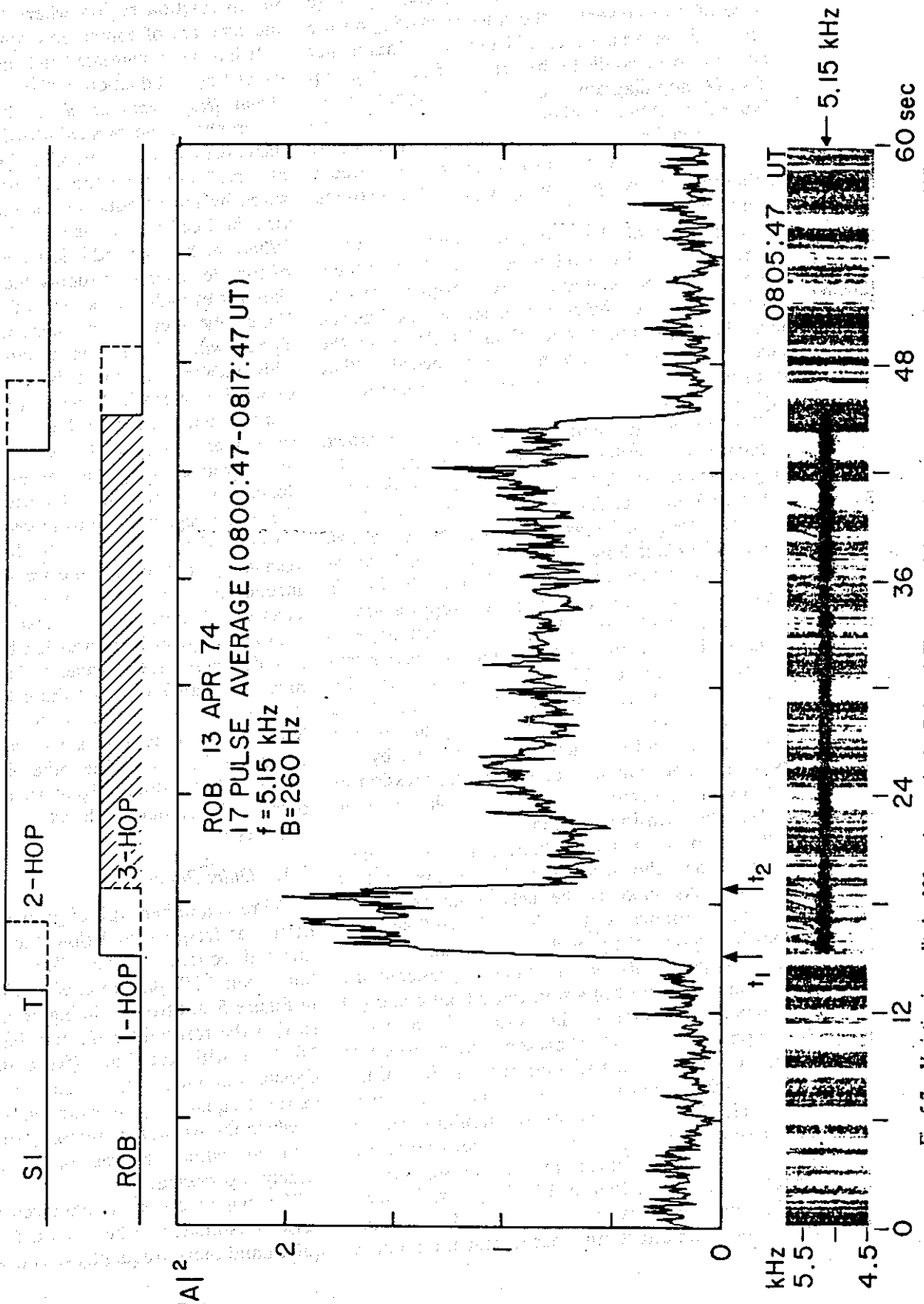

Fig. 5.7. Variation in amplitude of 30-s pulses received at Roberval. The top panel shows the time sequence of the various hops. The middle panel shows the square of the amplitude as a function of time. The plot is a 17-pulse average. Echo-induced suppression is seen in the form of a reduction in amplitude 4.0 s from the start of the pulse. The bottom panel shows the frequency-time spectrogram of a typical pulse from this time interval. Echo-induced suppression is again clearly seen. See text for an explanation of t_1 and t_2.

4 s the amplitude suddenly drops by about 3 dB (a factor of 2 in power) at the time marked t_2 on the record. From analysis of whistlers it is found that this time corresponds to the arrival of the three-hop echo. (A hop diagram is shown in the upper part of Figure 5.7.) After another period, corresponding to the two-hop time, the amplitude recovers somewhat, as can be seen on the record. There are subsequent oscillations whose periodicity equals the two-hop travel time.

At the end of the 30-s pulse there is a rapid decay to the noise level with no evidence of the echo which is postulated to have caused the growth suppression. Thus the echo intensity is less than the noise level, placing it more than 20 dB below the peak signal growth shown on the record. Other measurements give values of growth suppression as high as 20 dB.

The narrow band nature of suppression is shown in Figure 5.8, similar to Figure 5.7 except that the long pulses (now 31 s in length) alternate between 5.90 and 5.65 kHz. The amplitudes of the signals at these two frequencies are shown in the lower two panels. The first long pulse shows suppression at the two-hop travel time, as in Figure 5.7. In this case, however, the magnitude of suppression is much higher (~15 dB). The main feature appears at the end of the first pulse when the carrier frequency is lowered by 250 Hz. The initial intensity returns to about the same level as it was at the beginning of the first pulse, confirming that growth at a frequency 250 Hz lower is unaffected by the first pulse. The similarity of growth suppression at these two frequencies shows that the phenomenon is relatively insensitive to frequency.

Other experiments show that suppression occurs wherever the echo appears, including the start of the pulse. As soon as the echo (and associated emissions) terminates, the signal immediately resumes its exponential growth to saturation.

These experiments show that (1) suppression may occur during any part of a transmitted pulse and (2) suppression is limited to the period of time when the suppressing signal is present. Suppression is highly repeatable, occurring on at least 30% of the days on which transmitter signals are detected at Roberval. Thus the reduction in amplitude cannot be caused simply by destructive interference between two waves. Furthermore, the suppressing signal, as shown in Figure 5.7, is generally much weaker than the signal being suppressed. Therefore the suppression effect must occur near the input to the interaction region where the direct signal the echo are of comparable amplitude.

It has been suggested that growth suppressi caused by a reduction in the coherence of the signal [*Raghuram et al.*, 1977*b*]. A measur coherence is the bandwidth of the total signa the case of a signal consisting simply of two sinus of equal amplitude the coherence would be r sured by their frequency separation, or its reci cal, the beat period, as was discussed in sectio When the beat period is less than the bunching t of the electrons that supply the energy for grov then the growth rate is reduced. On the other ha if the frequency separation is sufficiently large, b signals will behave independently of one anotl This means that there is a range of freque separation over which the suppression effect will a maximum. Theoretical considerations and ot experiments suggest that suppression is maxim for a frequency spacing of the order of 50 H Spectral measurements of these records show tl the output signal contains many emissions coveri a range of the order of 50 Hz above the carr frequency. This causes the wave train to be higl incoherent from the point of view of the resona electrons. Hence phase bunching is inhibited.

How can growth suppression be avoided or mi mized? Figure 5.8 provides a clue. The modulati must be arranged so that the echo does not fall the signal. One method is to choose the spaci between the direct signals so that the echoes fall the space between. The other is to vary the fr quency of the direct signal so that the echo fal outside the frequency band in which suppressio can occur.

5.4. *Quiet Bands*

There is another type of growth suppression tha occurs at frequencies below the frequency of th injected coherent signal. This effect, called th 'quiet band' [*Raghuram et al.*, 1977*a*], is illustrate in Figure 5.9. Strong echoing occurred on this day so that the transmitter frequencies were essentiall filled in with the FSK (frequency shift keying signals and their echoes. Just below each of the carrier frequencies is a white band on the spectrum in which the natural magnetospheric noise generally seen throughout the rest of the record has been largely suppressed.

The magnitude of the observed reduction in the noise is estimated to be at least 6 dB. Below each quiet band there frequently occurs an enhancement

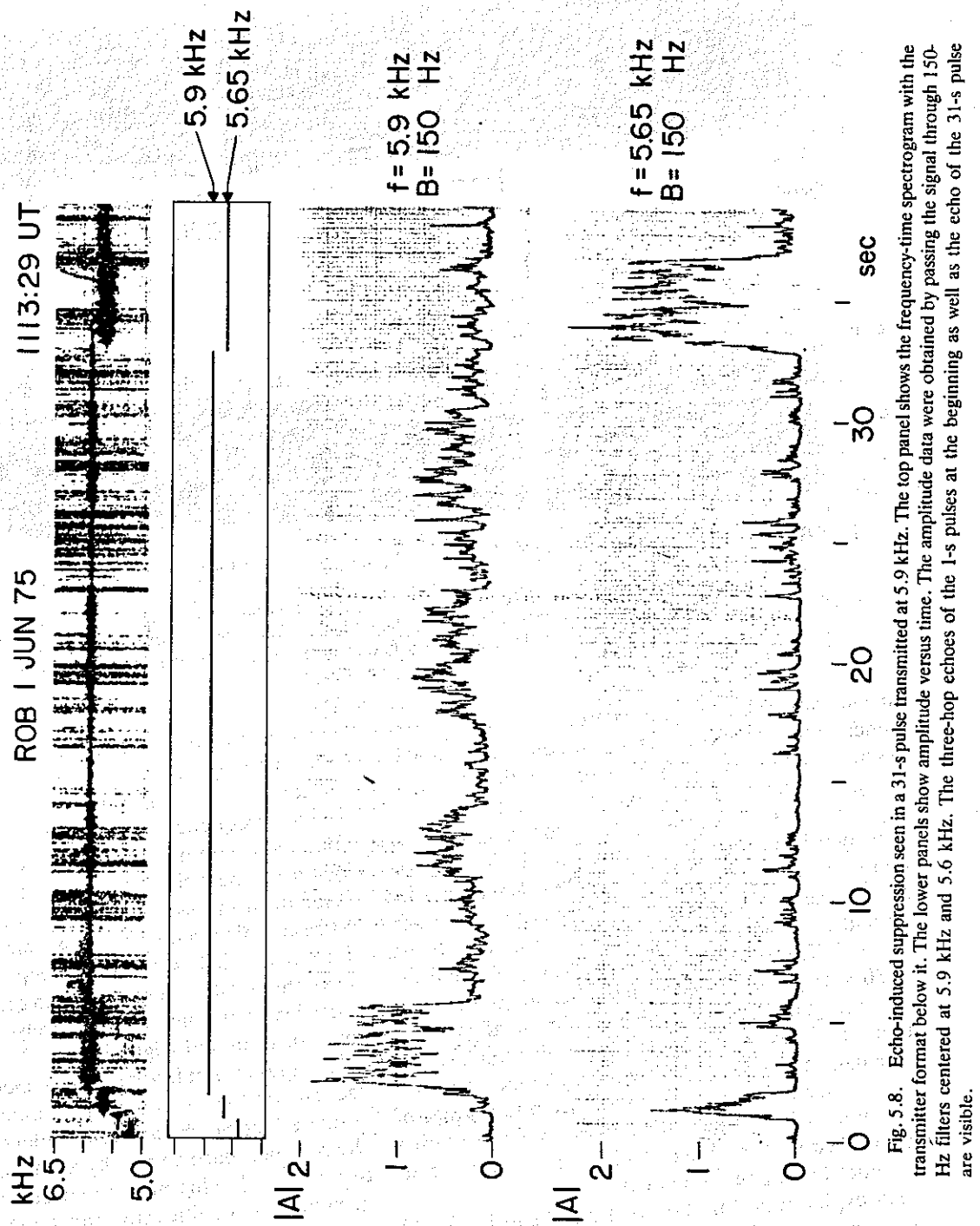

Fig. 5.8. Echo-induced suppression seen in a 31-s pulse transmitted at 5.9 kHz. The top panel shows the frequency-time spectrogram with the transmitter format below it. The lower panels show amplitude versus time. The amplitude data were obtained by passing the signal through 150-Hz filters centered at 5.9 kHz and 5.6 kHz. The three-hop echoes of the 1-s pulses at the beginning as well as the echo of the 31-s pulse are visible.

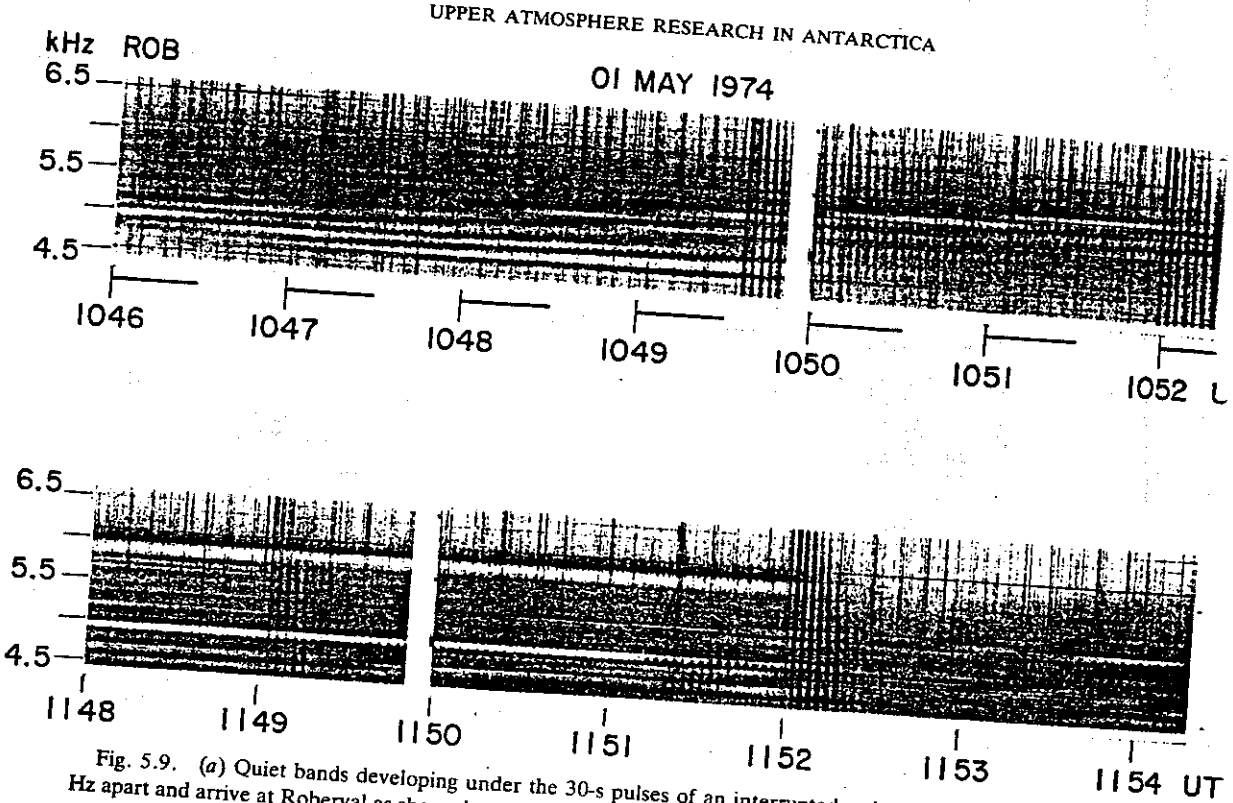

Fig. 5.9. (*a*) Quiet bands developing under the 30-s pulses of an interrupted staircase. The pulses are spaced 100 Hz apart and arrive at Roberval as shown by the 30-s line segments below the spectrum. (*b*) FSK sequence of 1-s pulses on 4.95 kHz and 5.95 kHz that terminates at 1152 UT. Below each signal is a quiet band that continues for about 30 s beyond the termination of the signals.

in intensity, as shown in Figure 5.9. Similar quiet bands and associated enhancements also appear below some of the many PLR lines in Figure 5.9.

An important feature of the quiet band that separates it from echo-induced growth suppression is a significant time lag in the quiet band development and recovery. It is found that the quiet band requires several seconds to develop after signal turn-on and an even longer time to recover after signal turn-off. The recovery time is typically of the order of 30 s or greater. These times are long compared with the growth time, which is almost always less than 1 s. Thus we must look for a different type of explanation from one involving a change in coherence of the total signal. (An earlier observation of the suppression of periodic emissions by preceding periodic emissions [*Brice*, 1964] may be related to the quiet band phenomenon.)

An explanation for the quiet band can be found in the process of particle scattering by the carrier wave and its triggered emissions. If we follow the amplified waves and their emissions as they leave the interaction region near the equator, we see that they interact with particles (with different energies) all along the field line. As the waves move away from the equator, the required parallel velocity for particles to be resonant increases because of t increasing gyrofrequency (see (3.2)). The wav scatter the resonant particles in pitch angle over narrow frequency band. The number of particl contained within this band is accordingly reduce When the particles arrive at the equator, they wi resonate with lower-frequency waves because of th corresponding reduction in gyrofrequency. Thus i a band just below the frequency of the perturbin wave there will be a reduction in the flux of resonan particles that may in turn cause a reduction ir amplification and triggering.

Computer simulations of this mechanism have in fact shown the existence of a relatively strong scattering effect which can easily reduce the intensity of the resonant particle flux by as much as 30% [*Raghuram*, 1977]. This may be sufficient to reduce the growth rate significantly and hence account for a reduction in the natural noise level. The noise peak just below the quiet band may be the result of an enhanced particle flux caused by the scattering, together with the presence of a power line harmonic that can serve as a frequency-controlled input signal. Another factor that influences growth and is affected by scattering is the anisotropy of the electron distribution function. Although the quiet band phenome-

non is seen infrequently, its startling characteristics provide an important new source of information on wave-particle interactions.

5.5 *Wave-Wave Interactions*

One of the fascinating aspects of Siple transmitter results is the general class of events that we have called wave-wave interactions. There are basically two classes of wave-wave interactions. In the first, new frequencies are triggered by an input signal as in Figure 5.1. In the second class, two independent signals come together in frequency, and one is entrained by the other. Entrainment may be followed in turn by triggering, which in turn may be followed by another entrainment, and so on. The process of successive triggering and entrainment can cause a self-excited oscillation to last a remarkably long time. Some triggered emissions have been observed to last as long as 30 or 40 s [*Helliwell*, 1965].

An example of the second class of wave-wave interactions is shown in Figure 5.10 (Figure 6 of *Helliwell and Katsufrakis* [1974]), in which an artificially stimulated emission (ASE) is entrained by PLR. The first Siple transmitter pulse on 5.0 kHz triggers an emission that initially falls in frequency. This self-excited oscillation then changes its frequency slope several times during its roughly 3.5-s lifetime. Five of the changes in slope are reversals in sense, between rising and falling. Induction lines of the local power system are clearly associated with the more prominent changes in slope. A second ASE, also showing changes in slope, is triggered by the fourth pulse on 5.0 kHz. Just before it terminates at about 4.6 s, its intensity is sharply reduced at an induction line. Although this ASE crossed the first at roughly 3.8 s, the two do not interact because they followed separate paths through the magnetosphere.

Another example of entrainment is shown in Figure 5.11. The transmitted signal consists of a staircase sequence of constant frequency signals, spaced 200 Hz apart, as shown in the lower panel. The triggered falling tones do not cross the next lower pulse but are entrained by that pulse without loss of intensity. Especially striking is the evident lack of growth of the 2-s pulse at 2.5 kHz in the top panel. Then when the faller from the preceding pulse encounters this 2-s pulse, the intensity is suddenly enhanced. The subsequent riser then is entrained by the first pulse of the up staircase, after which the entrainment chain is broken. In the middle panel the chain breaks at the last pulse of the down staircase, after which the pulses are relatively weak until the up staircase reaches 3.3 kHz. (Additional examples of entrainment are clearly evident in Figure 5.4.)

A small-scale version of the entrainment chain of Figure 5.11 can be found in Figure 5.4, where PLR lines play the role of the Siple transmitter. The clearest example is seen on the trace of the self-excited emission that is triggered at 5.3 s by a ramp starting at 4 s in the lower panel. At first the triggered emission falls slowly in frequency, becoming entrained at the fifty-ninth harmonic (3540 Hz) of 60 Hz. Then it steps up suddenly to approximately the sixty-first harmonic (120 Hz higher), where it is entrained for about 100 ms. There are two more upward steps, similar except that their spacing is nearer 60 Hz. Much of the irregularity in the traces of ASE's can probably be attributed to such partial entrainment by power system harmonic radiation.

We have seen that constant frequency signals

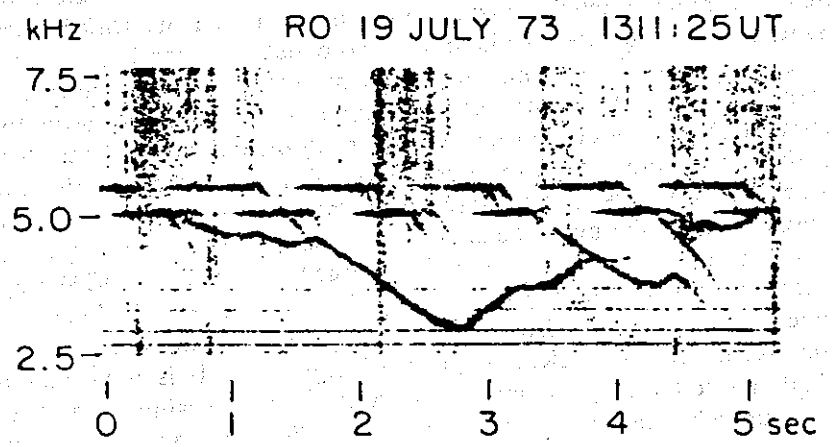

Fig. 5.10. Hooks triggered at 5.0 kHz show inflections and reversals in slope at power line harmonics, defined by the horizontal lines.

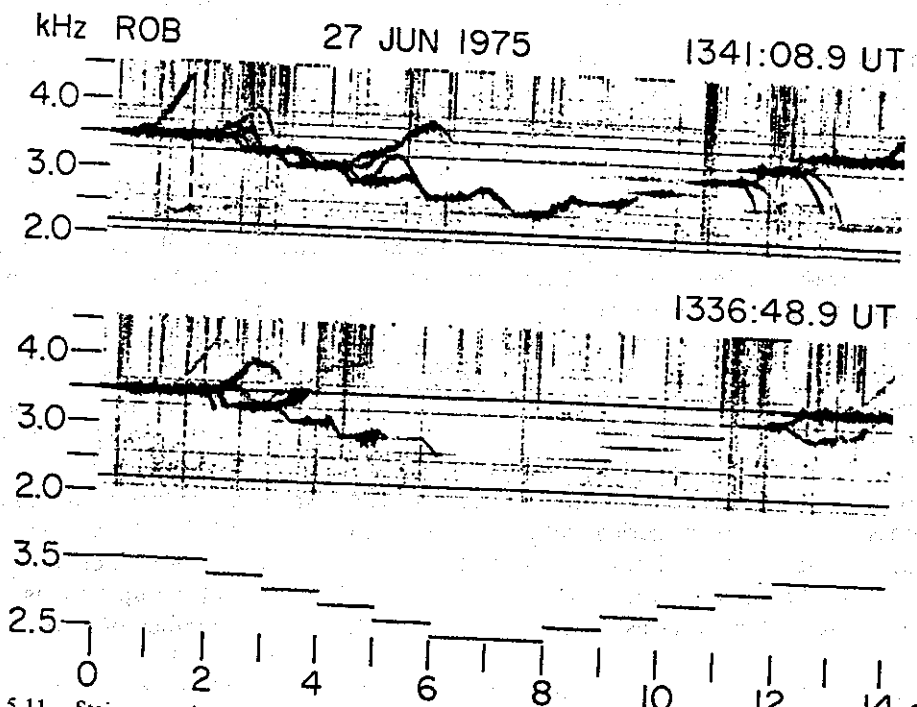

Fig. 5.11. Staircase pulses, whose pattern is shown in the lower panel, trigger fallers and inverted hooks that are entrained by the next pulse, as shown in the middle and top panels.

from the transmitter and from power systems can entrain free-running emissions. It is also common to observe entrainment by ramps, as illustrated in Figure 5.12. Several paths are evident, but on only two are there significant emissions. In all three panels the rising ramps on one of the paths trigger inverted hooks that become entrained by the next ramp, forming a scallop pattern. In the bottom panel a second path triggers only risers, which cross the entrained inverted hooks of the other path. At the point of crossing there is no evident interaction between the two emissions, suggesting negligible coupling between the two interaction regions. Other examples of noninteracting crossing emissions from separate paths can be seen in the upper two panels and also in Figure 5.4. Entrainment by ramps gives further support to the theoretical prediction that interaction physics should not be sensitive to df/dt.

During the period between the encounter of the self-excited emission with the transmitter pulse and the termination of the pulse the self-excited oscillation is effectively locked to the ramp frequency. The entrainment by the transmitter pulse is more definite than that by the PLR of Figure 5.10. The reason may be that the PLR, being a steady signal, had had time to build up an emission spectrum that reduces the coherence of its wave form. Its ability to synchronize another oscillation would then be reduced.

The process of entrainment maintains the amplitude of the strong self-excited oscillation, even though the frequency slope is changed. According to the theory described earlier, the falling and rising tones should be generated on opposite sides of the equator. Entrainment occurs too rapidly to be explained by drift of the interaction region from the falling tone location to the rising tone location, a distance of several thousand kilometers in most cases. The conclusion then is that the region of growth of the captured oscillation does not move but its df/dt is changed to that of the input signal. According to this theoretical model, the length of the interaction region must then be reduced. A possible reason for the amplitude to remain unchanged is that the input signal provides a portion of the end-fire array energy that is required to maintain the oscillation. Thus although the interaction region is reduced in length for the rising tone, it is still sufficiently long to maintain the amplitude that has already been established by the natural falling tone.

It is important to note the difference between entrainment and suppression. In entrainment there is only one external signal, so that the natural

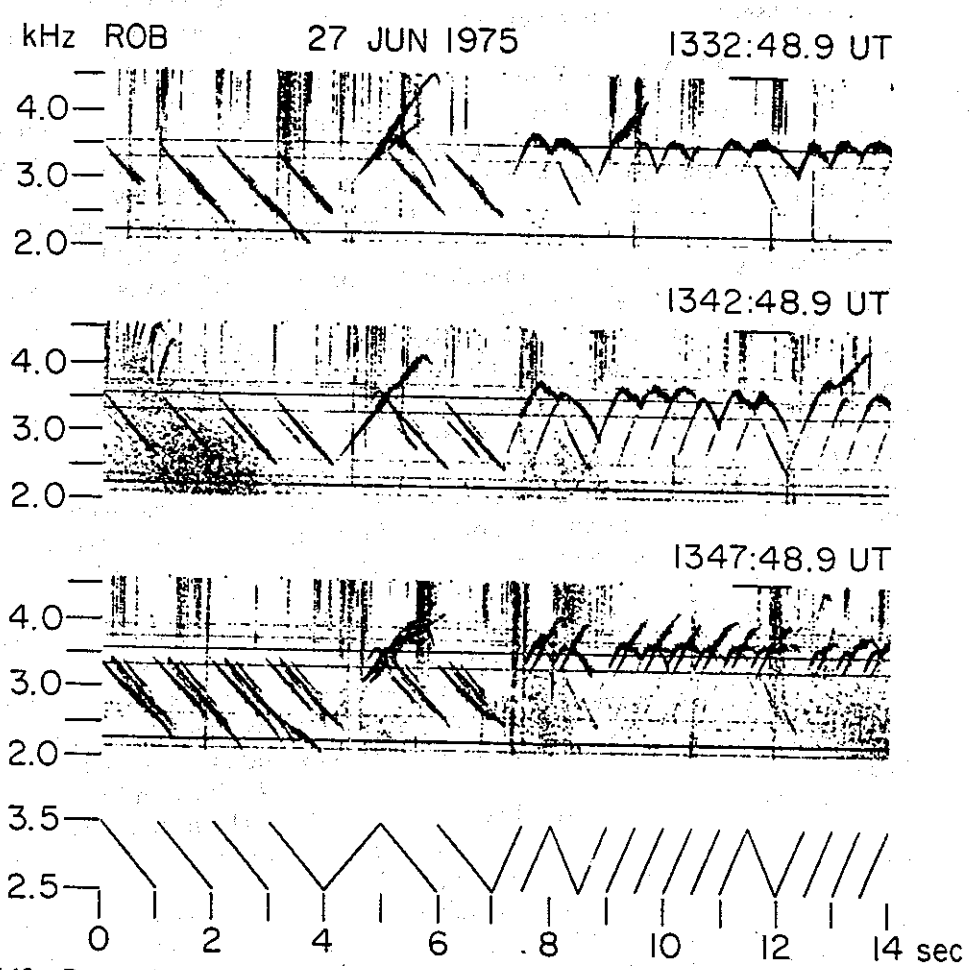

Fig. 5.12. Ramp pulses, whose pattern is shown in the lower panel, trigger inverted hooks that are entrained by the next pulse on the same path. The risers in the 1347:48.9 UT panel appear mainly on two paths. The inverted hooks triggered on the first path cross without interaction with the risers triggered on the second path, proof that the two corresponding interaction regions are uncoupled.

oscillator can change its frequency easily. In suppression, both signals are injected from the outside, and hence the total input wave must always be the sum of two external signals. Thus coherency can be maintained in entrainment but not in suppression.

5.6. *Satellite Observations of Siple Signals*

Signals from the Siple transmitter travel in the magnetosphere in both ducted and nonducted modes, as is illustrated in Figure 1.1. Although the nonducted mode is seldom if ever observed on the ground (because of the high wave normal angles), it accounts for perhaps 90% of the energy that enters the magnetosphere. It is important therefore to study its role in wave-particle interactions. The polar orbiting satellites Isis 2, Explorer 45, and Imp 6 have been employed to record Siple signals, showing amplification, triggering, multipath propagation, large Doppler shifts (up to 300 Hz), and plasmapause effects [*Bell and Inan,* 1975]. Strong signals have been seen throughout that portion of the magnetosphere that maps roughly into a circular area of 500-km radius centered on Siple Station.

The Imp 6 satellite has received nonducted Siple signals just outside the plasmapause (at $L = 4.15$) at a geocentric distance of about 5 R_E [*Inan et al.*, 1977*a*]. Signal intensity does not depend on pulse length, indicating negligible temporal growth. Ray path analysis of the group travel time from Siple to the satellite based on an independently derived model gives good agreement with the measurements [*Inan et al.*, 1977*b*]. Perturbations in the travel time data led to the identification on the plasmapause of a small ledge that was acting as a one-sided duct. These experiments are aiding the planning of future wave-particle experiments using Inter-

national Sun Earth Explorer satellites in which the Siple transmitter will play a key role.

6. FUTURE DIRECTIONS OF RESEARCH

The findings reported above have opened up a new avenue of study of upper atmosphere physics. Much more needs to be done to reveal and understand all of the intricate wave and particle phenomena of interest.

It is necessary to employ a more flexible modulation scheme so that the full spectrum of wave-wave interactions can be studied by using a single experimental transmitter. (Plans are under way to install a new transmitter at Siple that can accept any modulation pattern.) For example, we can study the role of coherence by measuring the growth rate and coupling of two signals as a function of their frequency separation. This would be done as a function of time and at different signal levels. We must also determine the effect of transmitter power on the maximum signal output and the growth rate. This requires a transmitter which can transmit amplitude-modulated waves. (In the present transmitter, each power change requires a period of at least several seconds during which changes in conditions may occur.)

Implied in this discussion is a knowledge of path location and electron density. This information can best be obtained by using whistlers, as described in chapter 4. To reach a full understanding of wave-particle interactions, we shall need coordinated passive and active experiments together with a variety of supporting experiments.

There are many possible future applications of active experiments. The ground-based active experiment on wave growth and ASE's is capable of giving data on the flux of energetic particles in the magnetosphere, thus reducing the need for satellite monitoring. Another application is the use of wave-induced precipitation to modify the magnetosphere and the ionosphere. The ability to control precipitation should be of great value in further studies of our atmospheric environment. With the VLF transmitter we expect to produce controlled amounts of precipitation with sudden onset times, giving in effect the transient response of the ionosphere. By varying the frequency of the wave we can control the altitude at which the precipitating particles are absorbed.

Another application of particular interest is the excitation of ULF (~1 Hz) waves by electron precipitation induced by VLF waves. In a recent study it was found that Pc 1 events (trains of ULF wave packets) were more numerous during Siple V transmissions than at other times [*Fraser-Smith a Cole,* 1975]. It is supposed that the VLF wa precipitate energetic electrons into the ionosphe by pitch angle scattering and enhance ionization *D* and *E* region altitudes. This increased ionizati causes a conductivity increase, which in turn mod lates the horizontal current driven by the in si electric field. The varying current then launch ULF waves up the field lines, which may then b amplified by cyclotron resonant streams of proto in a manner analogous to the growth of VLF wav by electrons [*Brice,* 1964]. A quantitative model the excitation process shows that the observed am plitudes of VLF waves should be sufficient to pro duce detectable ULF waves [*Bell,* 1976].

New techniques will be needed to observe th effects of wave-induced precipitation. To detec >30-keV electrons, reaching below 90 km, we ca use X rays, riometer data, and VLF propagatio perturbations as outlined in section 2. Signal integration techniques will be useful in enhancing the sensitivity of these methods. Another method is to use the ionosonde to measure absorption and to observe sporadic *E* and other transient ionization. A direct and powerful method is to use rockets to make in situ measurements of the incident electron fluxes over the transmitter.

Ultimately, one can expect that the ground-based VLF transmitter will lead to similar experiments performed by using a transmitter on board a satellite. A satellite-borne transmitter at VLF has the advantage of exciting a wider range of wave normals than is accessible to a ground-based source. The reason is that the large refractive index of the ionosphere at VLF causes all input waves from the ground to be refracted into a relatively small transmission cone. In addition, a satellite transmitter of suitable power, say, several thousand watts, is capable of creating much larger field intensities than are practical from ground transmitters.

VLF wave injection experiments may lead to new communication systems. We have shown that VLF signals themselves can be amplified 3 orders of magnitude in power, giving an effective transmitter power of 1 MW for a radiated power of only 1 kW. The ability to control precipitation could provide a new communication technique at ULF (~1 Hz), as discussed earlier.

Finally, we note that many of the phenomena described in this chapter have not yet been identified in the laboratory. Thus controlled wave-particle interaction experiments in the magnetosphere can

provide useful input to fundamental laboratory plasma physics.

Acknowledgments. We would like to acknowledge the valuable support of our antarctic activities provided by the Division of Polar Programs of the National Science Foundation, the U.S. Navy, and Holmes and Narver, Inc. We are grateful to the Atmospheric Sciences Section of the National Science Foundation for support of our field operations at Roberval, Quebec, Canada, and wish to thank the Office of Naval Research for providing a solid state VLF transmitter that was modified for the scientific program at Siple Station.

REFERENCES

Bell, T. F., ULF wave generation through particle precipitation induced by VLF transmitters, *J. Geophys. Res., 81,* 3316, 1976.

Bell, T. F., and U. S. Inan, Satellite observations of nonducted signals from the Siple transmitter, *Antarctic J., X*(5), 211, 1975.

Brice, N. M., An explanation of triggered very low frequency emissions, *J. Geophys. Res., 68,* 4626, 1963.

Brice, N. M., Fundamentals of very low frequency emission generation mechanisms, *J. Geophys. Res., 69,* 4515, 1964.

Cornwall, J. M., Scattering of energetic trapped electrons by very low frequency waves, *J. Geophys. Res., 69,* 1251, 1964.

Dingle, B., The electron flux precipitated by wave bursts in the magnetosphere, submitted to *J. Geophys. Res.*, 1977.

Dungey, J. W., Resonant effect of plasma waves on charged particles in a magnetic field, *J. Fluid Mech., 15,* 74, 1963.

Fraser-Smith, A. C., and C. A. Cole, Jr., Initial observations of the artificial stimulation of VLF pulsations by pulsed VLF transmissions, *Geophys. Res. Lett., 2,* 146, 1975.

Helliwell, R. A., *Whistlers and Related Ionospheric Phenomena,* Stanford University Press, Stanford, Calif., 1965.

Helliwell, R. A., A theory of discrete VLF emissions from the magnetosphere, *J. Geophys. Res., 72,* 4773, 1967.

Helliwell, R. A., Intensity of discrete VLF emissions, in *Particles and Fields in the Magnetosphere,* edited by B. M. McCormac, pp. 292–301, D. Reidel, Hingham, Mass., 1970.

Helliwell, R. A., and T. L. Crystal, A feedback model of cyclotron interaction between whistler mode waves and energetic electrons in the magnetosphere, *J. Geophys. Res., 78,* 7357, 1973.

Helliwell, R. A., and E. Gehrels, Observations of magneto-ionic duct propagation using man-made signals of very low frequency, *Proc. IRE, 46*(4), 785, 1958.

Helliwell, R. A., and J. P. Katsufrakis, VLF wave injection into the magnetosphere from Siple Station, Antarctica, *J. Geophys. Res., 79,* 2511, 1974.

Helliwell, R. A., J. Katsufrakis, M. Trimpi, and N. Brice, Artificially stimulated VLF radiation from the ionosphere, *J. Geophys. Res., 69,* 2391, 1964.

Helliwell, R. A., J. P. Katsufrakis, and M. L. Trimpi, Whistler-induced amplitude perturbation in VLF propagation, *J. Geophys. Res., 78,* 4679, 1973.

Helliwell, R. A., J. P. Katsufrakis, T. F. Bell, and R. Raghuram, VLF line radiation in the earth's magnetosphere and its association with power system radiation, *J. Geophys. Res., 80,* 4249, 1975.

Helms, W. J., H. M. Swarm, and D. K. Reynolds, An experimental study of the polar lower ionosphere using very low frequency radio waves, *Tech. Rep. 123,* Dep. of Elec. Eng., Univ. of Wash., Seattle, May 1968.

Inan, U. S., T. F. Bell, and R. R. Anderson, Cold plasma diagnostics using satellite measurements of VLF signals from ground transmitters, *J. Geophys. Res., 82,* 1167, 1977*a*.

Inan, U. S., T. F. Bell, D. L. Carpenter, and R. R. Anderson, Explorer 45 and Imp 6 observations in the magnetosphere of injected waves from the Siple Station VLF transmitter, *J. Geophys. Res., 82,* 1177, 1977*b*.

Jørgensen, T. S., Interpretation of auroral hiss measured on Ogo 2 and at Byrd Station in terms of incoherent Cerenkov radiation, *J. Geophys. Res., 73,* 1055, 1968.

Kennel, C. F., and H. E. Petschek, Limit on stably trapped particle fluxes, *J. Geophys. Res., 71,* 1, 1966.

Maggs, J. E., Coherent generation of VLF hiss, *J. Geophys. Res., 81,* 1707, 1976.

McPherson, D. A., H. C. Koons, M. H. Dazey, R. L. Dowden, L. E. S. Amon, and N. R. Thomson, Conjugate magnetospheric transmissions at VLF from Alaska to New Zealand, *J. Geophys. Res., 79,* 1555, 1974.

Nunn, D., A self consistent theory of triggered VLF emissions, *Planet. Space Sci., 22,* 349, 1974.

Raghuram, R., Suppression effects associated with VLF transmitter signals injected into the magnetosphere, *Tech. Rep. 3456-3,* Radiosci. Lab., Stanford Electron. Lab., Stanford Univ., Stanford, Calif., March 1977.

Raghuram, R., R. L. Smith, and T. F. Bell, VLF Antarctic antenna: Impedance and efficiency, *IEEE Trans. Antennas Propagat., AP-22,* 334, 1974.

Raghuram, R., T. F. Bell, R. A. Helliwell, and J. P. Katsufrakis, A quiet band produced by VLF transmitter signals in the magnetosphere, *Geophys. Res. Lett., 4,* 199, 1977*a*.

Raghuram, R., T. F. Bell, R. A. Helliwell, and J. P. Katsufrakis, Echo-induced suppression of VLF transmitter signals in the magnetosphere, *J. Geophys. Res.*, 2787, 1977*b*.

Rosenberg, T. J., R. A. Helliwell, and J. P. Katsufrakis, Electron precipitation associated with discrete very low frequency emissions, *J. Geophys. Res., 76,* 8445, 1971.

Siren, J. S., Fast hisslers: A form of magnetospheric radio emissions, *Tech. Rep. 3464-1,* Radiosci. Lab., Stanford Electron. Lab., Stanford Univ., Stanford, Calif., Aug. 1974.

Stiles, G. S., Digital spectra of artificially stimulated VLF emissions, *Tech. Rep. 3465-3,* Radiosci. Lab., Stanford Electron. Lab., Stanford Univ., Stanford, Calif., 1974.

Stiles, G. S., and R. A. Helliwell, Frequency-time behavior of artificially stimulated VLF emissions, *J. Geophys. Res., 80,* 608, 1975.

Stiles, G. S., and R. A. Helliwell, Stimulated growth of coherent VLF waves in the magnetosphere, *J. Geophys. Res., 82,* 523, 1977.